



SCHOOL of
GRADUATE STUDIES
EAST TENNESSEE STATE UNIVERSITY

East Tennessee State University
Digital Commons @ East Tennessee
State University

Electronic Theses and Dissertations


Student Works

5-2021

Theranostic Nanoparticles Folic Acid-Carbon Dots-Drug(s) for Cancer

Godwin Kweku Babanyinah
East Tennessee State University

Follow this and additional works at: <https://dc.etsu.edu/etd>

 Part of the [Analytical Chemistry Commons](#), [Medicinal-Pharmaceutical Chemistry Commons](#), and the [Organic Chemistry Commons](#)

Recommended Citation

Babanyinah, Godwin Kweku, "Theranostic Nanoparticles Folic Acid-Carbon Dots-Drug(s) for Cancer" (2021). *Electronic Theses and Dissertations*. Paper 3892. <https://dc.etsu.edu/etd/3892>

This Thesis - unrestricted is brought to you for free and open access by the Student Works at Digital Commons @ East Tennessee State University. It has been accepted for inclusion in Electronic Theses and Dissertations by an authorized administrator of Digital Commons @ East Tennessee State University. For more information, please contact digilib@etsu.edu.

Theranostic Nanoparticles Folic Acid-Carbon Dots-Drug(s) for Cancer

A thesis

presented to

the faculty of the Department of Chemistry

East Tennessee State University

In partial fulfillment

of the requirements for the degree

Master of Science in Chemistry

by

Godwin Kweku Babanyinah

May 2021

Dr. Hua Mei, Ph.D., Chair

Dr. Greg Bishop

Prof. Catherine McCusker

Keywords: carbon dots, doxorubicin, gemcitabine, targeted drug delivery, cancer therapy

ABSTRACT

Theranostic Nanoparticles Folic Acid-Carbon Dots-Drug(s) for Cancer

by

Godwin Kweku Babanyinah

This study aims to prepare theranostic nanoparticles (NPs) that are expected to increase cancer diagnostics and therapeutic efficacy. We prepared the NPs constituting carbon dots (CDs) as an imaging agent, folic acid as a targeting agent, doxorubicin (DOX), or gemcitabine (GEM) as chemotherapy agents. The NPs include noncovalent FA-CDs-DOX, covalent CDs-FA-DOX, and covalent FA-CDs-GEM. Through ultraviolet-visible spectroscopy, fluorescence spectroscopy, and Fourier transform-infrared spectroscopy, the fabrication of these NPs was confirmed. It was discovered that the high drug loading efficiency is the noncovalent series while the high drug loading capacity is the covalent series. The in-vitro pH-dependent drug release data indicate the NPs release more drugs at around pH 5.0 than at pH 7.4. The NPs sizes are between 2-5 nm. The Cell viability was investigated using the Alamar Blue assay and the three NPs complexes exhibited strong therapeutic efficacy against MDA-MB-468 breast cancer cells as compared with CDs-drug.

Copyright 2021 by Godwin Kweku Babanyinah
All Rights Reserved

TABLE OF CONTENTS

ABSTRACT.....	2
LIST OF TABLES	6
LIST OF FIGURES	7
LIST OF SCHEMES.....	9
LIST OF ABBREVIATIONS.....	10
CHAPTER 1. INTRODUCTION	11
Cancer Treatment and Early Detection	11
Chemical Therapy.....	14
Nanosized Drug Delivery System for Chemical Therapy	15
Quantum Dots.....	19
Carbon Dots.....	20
Carbon Dots as DDS.....	21
CDs for Cancer Cell Detection.....	22
Carbon Dots Synthesis.....	23
Target Agent	24
Folic Acid	25
Cocktail Chemotherapy	26
Doxorubicin (DOX).....	27
Gemcitabine (GEM)	28
Research Plan	30
CHAPTER 2. EXPERIMENTAL.....	32
General Material	32
Synthesis of CDs	32
Synthesis of Non-covalent CDs-DOX from DOX.HCl.....	33
Synthesis of Non-covalent FA-CDs-DOX from DOX.HCl	33
Synthesis of Covalent CDs-DOX or CDs-GEM from DOX.HCl or GEM.HCl	34
Synthesis of Covalent FA-CDs-DOX or FA-CDs-GEM From DOX.HCl or GEM.HCl.....	34
Spectroscopy.....	35
CHAPTER 3. RESULTS AND DISCUSSION.....	37
Synthesis of CDs	37

Covalent Synthesis of CDs-DOX/CDs-GEM Complexes.....	37
Synthesis Covalent of FA-CDs-DOX / FA-CDs-GEM Complexes.....	38
Calibration Curve for DOX	38
Calibration Curve for GEM.....	39
Drug Load Content (DLC) and Drug Load Efficiency (DLE)	40
UV-vis Analysis of Nanoparticles	41
Photoluminescence Analysis of Nanoparticle	45
FTIR for Nanoparticle	50
FTIR for GEM Nanoparticle	55
Drug Loading Profile.....	58
pH-sensitive Drug Release For Noncovalent FA-CDs-DOX.....	59
Cell Viability Assay.....	63
CHAPTER 4. CONCLUSION.....	66
REFERENCES	67
APPENDICES	81
<i>Appendix A: Standard Calibration and Drug Release Tables</i>	81
<i>Appendix B: Calculation of DLE and DLC Before Dialysis</i>	86
VITA.....	93

LIST OF TABLES

Table 1. Types of NPs DDS: Examples, Advantages, and Disadvantages.....	17
Table 2. Carbon Dots Synthetic Approach	24
Table 3. Drug Load Profile for Covalent and Noncovalent Complexes.....	41

LIST OF FIGURES

Figure 1. Global percentage estimation of new cases of all cancer in both sexes and all ages in 2018	11
Figure 2. Classification of anticancer agents	15
Figure 3. Different applications of Carbon Dots.	21
Figure 4. The structure of folic acid.....	26
Figure 5. Structure of DOX	28
Figure 6. Structure of GEM	30
Figure 7. Calibration curve of pure DOX.....	39
Figure 8. Standard curve of GEM.HCl showing concentration (in mg/mL) against absorbance at 269 nm	40
Figure 9. UV-vis of 0.01mg/ml CDs showing the peaks 198 nm, 240 nm, and 344 nm.....	42
Figure 10. UV-vis of 0.01 mg/ml CDs-DOX, FA-CDs-DOX, and DOX.	43
Figure 11. UV-vis spectra of obtained CDs (0.01mg/ml), CDs-GEM (0.01mg/ml), and 0.01mg/ml FA-CDs-GEM complex. The insert shows fluorescence spectra of CDs, CDs-GEM and FA-CDs-GEM excited at 360 nm.....	44
Figure 12. FL spectra of CDs (0.01 mg/mL). The inset at the upper-right corner shows a photograph of D.I water (left), and CDs in an aqueous solution (right) under visible light.....	46
Figure 13. FL spectra of 0.01mg/mL covalent DOX complexes.....	47
Figure 14. FL spectra of 0.01mg/mL covalent GEM complexes.	49
Figure 15. ATR-FTIR spectra of CDs	50
Figure 16. ATR-FTIR spectra of FA	51

Figure 17. ATR-FTIR spectra of pure DOX.....	52
Figure 18. ATR-FTIR spectrum of covalent CDs-DOX complex.....	53
Figure 19. ATR-FTIR spectrum of covalent FA-CDs-DOX (A) and noncovalent FA-CDs-DOX complex (B)	54
Figure 20. ATR-FTIR spectra of pure GEM	56
Figure 21. ATR-FTIR spectra of CDs-GEM (A) and FA-CDs-GEM (B).....	58
Figure 22. Graph showing the drug released in vitro at regular intervals at pH 5.0 and 7.4 phosphate-buffered saline (PBS).....	61
Figure 23. Graph showing the in vitro DOX released at regular intervals at pH 5.0 and 7.4 phosphate-buffered saline (PBS).....	62
Figure 24. Graph showing the in vitro GEM released at regular intervals at pH 5.0 and 7.4 phosphate-buffered saline (PBS).....	63
Figure 25. Cell viability of MDA-MB-468 cells exposed to free DOX, noncovalent CDs-DOX, and noncovalent FA-CDs-DOX at 72 h	64
Figure 26. Cell viability of MDA-MB-468 cells exposed to free DOX, covalent CDs-DOX, and covalent FA-CDs-DOX at 72 h	65

LIST OF SCHEMES

Scheme 1. Hydrothermal synthesis of CDs. The insert picture for CDs showed a brilliant blue solution under UV light.....	32
Scheme 2. EDC/NHS coupling reaction.....	35

LIST OF ABBREVIATIONS

CDR	Cumulative drug release
CDs	Carbon Dots
DLC	Drug load content
DLE	Drug load efficiency
DOX	Doxorubicin
EDC	3-(3-Dimethylaminopropyl)-1-ethyl-carbodiimide
FA	Folic Acid
FR	Folate receptor
FL	Fluorescence spectroscopy
FTIR	Fourier transform-infrared spectroscopy
GEM	Gemcitabine
NHS	N-Hydroxy succinimide
NPs	Nanoparticles
PBS	Phosphate Buffered Saline
QDs	Quantum Dots
UV-vis	Ultraviolet-Visible spectroscopy

CHAPTER 1. INTRODUCTION

Cancer Treatment and Early Detection

According to a report by the world health organization, there were 18 million cases of cancer with 9.6 million death globally in 2018. The report also indicated that one in every six death is due to cancer, making cancer the second leading cause of death. Some of the cancer types often diagnosed in America include lung cancer, breast cancer, prostate cancer, colorectal cancer, and breast cancer as shown in figure 1. ^{1, 2}

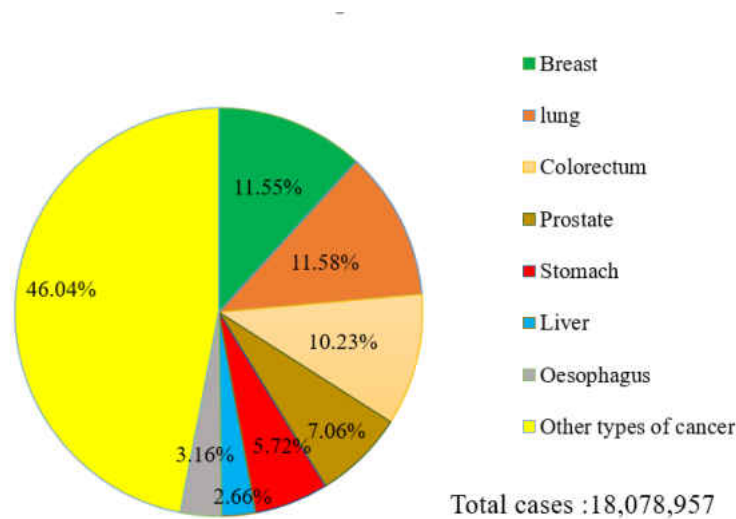


Figure 1. Global percentage estimation of new cases of all cancer in both sexes and all ages in 2018

There are several approaches to cancer treatment, such as surgical removal of cancer tissue, chemotherapy, immunotherapy, radiotherapy, hormone therapy, and cryoablation. Radiotherapy is one of the oldest methods in cancer treatment since the discovery of X-ray in 1895. Radiotherapy often causes side effects such as hair loss, fatigue, vomiting and nausea, and vomiting, and infertility in both men and women. The reason is that the radioactive elements are

used in radiotherapy, the healthy cells are affected by radiation making the radiotherapy less specific to targeting cancer cells.³ Another method, the surgical approach, is an intervention and prevention approach in curing individuals with cancer. However, after surgical removing cancer, sometimes cancer relapse occurs. According to the literature, the surgical approach often leads to the development of secondary malignant growth near the primary site of the tumor during the process of healing. It is also accompanied by the possibility of the accelerating growth of the remaining tumor cells. For example, it was documented that the surgical approach could lead to an increase in the cancer cells when detached cancer cells circulate in the body fluid.⁴ Moreover, it is difficult to completely remove all the cancer cells during surgical operations because the cancer cells are not fully differentiated from healthy cells.⁵

The capacity for early detection of cancer in an individual is important in the treatment and prevention of the disease. In many instances, cancer is not diagnosed until the cancer cells spread beyond the site of origin. With the early detection of cancers at preliminary stages, there will be a higher probability for the treatment and curing of the disease.⁶ Early detection has helped improve the treatments of cancer, which in the long run significantly increased survival rates. For cancer detection, the patients usually are screened for certain physical warning signs of the disease. A clinical test can also be performed to diagnose the disease. There are some early physical indications of cancer growth, including irregular bleeding, development of lumps, skin blemishes, and non-healing wounds. Many health agencies such as the American Cancer Society, the World Health Organization, and the Center for Disease Control educate and give recommendations to the general public, and healthcare providers on how to detect these early physical signs of cancer. For example, regular physical examination of the female breast for irregularities has become a common practice recommended by the American Cancer Society to

be conducted every three (3) years intervals for women between the age of 20 to 40 years old.⁷

Although the physical examination is nonconclusive to infer cancer development, it pre-informs the individual on the next step to confirm the presence or the absence of cancer growth. The further step in cancer detection and confirmation is through clinical screening.

Clinical screening usually provides scientific or clinical evidence of cancer or tumor growth. Clinical screening is, therefore, an effective diagnostic technique used in cancer detection. This involves conducting various clinical tests on an individual with or without any signs of cancer. Clinical screening often detects cancer antibodies and cell receptors present on cancer cell surfaces. For instance, for cervical, prostate, lung, and breast cancer diagnosis, cytological examination, or serological test is used to detect early-stage cancer development. This screening method mostly relies on detecting the relatively high concentration of certain cancer biomarkers such as alpha-fetoprotein (liver cancer), and BRCA2 (breast/ovarian cancer).⁸ Since the detectable biomarkers are produced in very low concentration during the early stages of cancer, their detection by this method is almost impossible and often gives false negative. This screening type has been used successfully in detecting cancer tumors, however, their ability to detect early stages of cancer is limited.^{7, 9, 10}

Another method of early cancer detection tool of clinical screening is called a whole-body scan that involves using high-energy radiation, electrons, or electromagnetic wave to directly visualize cancer in the body. The whole-body scanning tools include magnetic resonance imaging (MRI), X-rays, and positron emission tomography (PET). For example, mammography is a technique using X-rays to diagnose and locate lung or breast cancer. Because of high-energy radiation, ultrasound, and radioactive tracers, these tools pose some health risks. According to

the America College of Preventive Medicine, these methods are also difficult to detect deep tissue cancer cells, and costly, costing between \$500 to \$1,000.^{11,12,13}

Chemical Therapy

For many years, the use of chemotherapy (chemical agents) for cancer treatment has found grounds in recent pharmacological research. The chemical agents either inhibit the growth and or directly kills the cancer cells, thereby stopping the growth of the tumor.¹⁴ Different classes of cancer drugs have their unique mechanisms toward cancer cell destruction. Some anticancer drugs can impair the DNA or RNA synthesis in cancer cells by disrupting the process of the cancer cell division (mitosis and meiosis). Other classes of anticancer drugs block a specific vital metabolite that is required for cancer cell survival. When the cancer cells are deprived of their essential metabolite and cannot divide, they can no longer spread and eventually die. The anticancer drug also can be administered singularly or in combination with another. One of the typical classifications of cancer drugs is based on their working mechanism is shown in figure 2. Anticancer drugs usually are given to patients orally or intravenously. However, most cancer drugs are non-specific for cancer cells. Most anticancer drugs harm both the cancerous and the healthy cells which often leads to serious side effects. Such side-effects include; anemia, diarrhea, nausea and vomiting, and hair loss. This has become one of the main challenges in cancer chemotherapy. Chemotherapy has, therefore, not been able to reach its full potential.^{5,15,16}

The upsurge in cancer chemotherapy research is incited by finding solutions to this and other drawbacks pertaining to chemotherapy. The challenges facing many anticancer drugs needed to be resolved include drug selectivity, drug distribution, drug resistance, and drug solubility. Improving these areas of drug pharmacokinetic is reported to help enhance the cancer

drug circulation, distribution, release rate to the cancer site. The research into the drug delivery system (DDS) and its application in cancer chemotherapy have been explored widely.

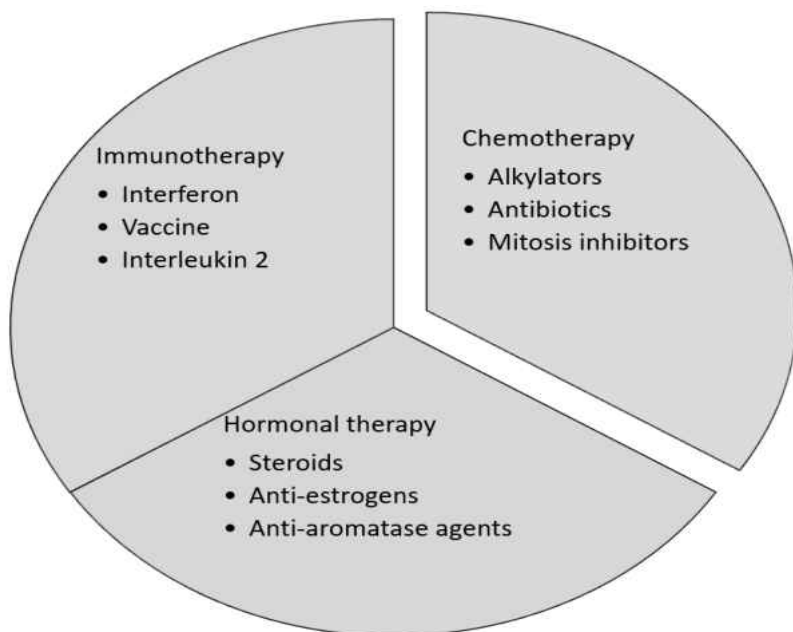


Figure 2. Classification of anticancer agents

Nanosized Drug Delivery System for Chemical Therapy

One of the main challenges in chemical therapy is to control release and site-specific delivering anticancer drugs. One way to resolve this drawback to achieve a higher therapeutic effect of administered chemical agents is by using delivering agents, also known as drug delivery systems (DDS). The use of DDS in therapy is known to improve the overall drug profile; bio-distribution, drug release, drug absorption, and elimination. This improvement is noted to increase the therapeutic benefits of drugs.

Among the different types of DDS, the nanosized DDS are known to significantly enhance the diffusion of the loaded drug into the specific cancer cells. With the sizes less than

100 nm, the nanosized DDS is easier to load drugs and aid them to cross tissue barriers. This improves the drug therapeutic efficiency since the overall cellular uptake is enhanced.¹⁷ Some common types of NPs DDS include liposomes, polymeric micelle, dendrimers, and mesoporous silica nanoparticles.

Nanosized-based DDS in cancer therapy is documented to overcome drug resistance. Drug efflux pumps on cancer cells are reported to participate in anticancer drug resistance by cancer cells. Free anticancer drugs are usually internalized through diffusion across the cell membrane. The drug efflux pumps present on many cancer cells membrane can detect the free anti-cancer drug and prevent them from getting into the cancer cell. According to Kibria Et al., to increase the drug efficacy, nanosized-based DDS can be a powerful tool where the drug can be loaded for delivery. This is because the nanosized-based DDS can cross the cell membrane using a non-specific endocytosis route that is undetectable by the efflux pumps resulting in a higher accumulation of the loaded anticancer drug with the cancer cells.^{18,19,20}

With the DDS, the therapeutic agent can be transported to the specific tissue site of action. This enables the drug to selectively interact with the cancer cells. Therefore, it alleviates some of the drug's side effects since the drug will not interact with the healthy tissues in the cancer microenvironment. Moreover, some specific DDS can keep the drug stable and prevent biodegradation or drug clearance from the body. Most importantly, the DDS can dramatically increase the drug effective concentration at the sites lowers the required dosage of drugs. Therefore, it results in low cytotoxicity and fewer side effects.^{5, 21 22 17} Table 1 summarizes the different types of DDS used in cancer research.^{23 24} The DDS includes polymers, transition metals, and carbon-based materials. Their advantages and disadvantages are as well summarized.

The method of loading the drug onto the DDS is very important as it affects the loading capacity, loading efficiency, and drug release of the DDS.

Table 1. Types of NPs DDS: Examples, Advantages, and Disadvantages

Type of DDS	Examples	Advantages & disadvantages
Polymer	Liposomes	It is biocompatible.
	Micelles	Nontoxic.
	Dendrimers	Have a relatively larger particle size.
	Microsphere	
Metal base	Au NP	Photo-fluorescence
	Palladium NP	Bio-incompatible
	Platinum NP	High toxicity
	Iron Oxide NP	
Carbon base	Nano-diamond	Biocompatible
	Carbon nanotube	
	Graphene oxide	
	Carbon dots	

Typically, the therapeutic agent(s) is chemically or physically attached to DDS. Physical attachment such as encapsulation is especially advantageous for targeting cancer cells. The lipid-mediated DDS with an encapsulated drug is reported to enhance the affinity of the drug with the cancer cell. Also, the common non-covalent bond observed between the drugs and DDS includes π - π interaction, hydrogen bonding, electrostatic, hydrophobic, and steric immobilization. This form of attachment results in the easy release of the loaded drug. However, the non-covalent interaction to those DDS can lead to comparably low drug loading content and efficiency.²⁵ Covalent bonding, usually involves the structural changes of the DDS and the

loaded drug to form the actual chemical bond such as the amide bond. With covalent attachment, the drug loading capacity and efficiency of the DDS is enhanced. Moreover, the covalent attachment of drugs to DDS makes it flexible to control the concentration of the drugs loaded onto the DDS. Nevertheless, it becomes difficult for the drug to be released once attached to the DDS.^{25, 26,19, 27}

Polymer NPs DDS is generally reported to be less or non-toxic and highly biocompatible. Nevertheless, many polymeric NPs used as DDS are reported to respond slowly to stimuli relative to other types of NPs. These stimuli comprise light, pH, and temperature. Since these stimuli are not specific to any organ or tissue in the body there is no specificity in the release drugs.²³ Moreover, the rather large size of many polymeric NPs DDS poses problems such as poor stability, absorption, bioavailability, and clearance. All these limits their biomedical applications.

Metal NPs DDS in cancer chemotherapy has also been developed in cancer-related research. Examples of the metal base NPs are; Au, Rh, Ir, and Pd.²⁴ Metal-based NPs are chosen because of their large surface area, broad optical properties, easily functionalized with different chemical groups. Nevertheless, these NPs as DDS are also limited in their application in biomedical research. Metal-based NPs are reported to have high cellular toxicity and short-lived photoluminescence for bioimaging. Depending on the metal and how the NPs are made, it is usually very simple and often required that the NP will have functional groups. Bare metal nanoparticles are often difficult or impossible to prepare as a suspension because capping agents are often required for a successful bottom-up approach. This, therefore, limit their drug loading capacity.²⁸ Hence, considerable biomedical research is shifted toward finding alternative NPs

DDS that have less cellular toxicity, high biocompatibility, more flexibility for chemical functionalization, and free of heavy metal.

One of the most common NPs DDS that has attracted attention is carbon-based NPs due to their inherent characteristics such as excellent water solubility, high photostability, chemical inertness, and long lifetime emission. The typical examples of the carbon-based NPs DDS are single or multi-walled carbon nanotubes, graphite, fullerene, nano-diamond, and carbon dots.¹⁴

Quantum Dots

Quantum dots (QDs) are inorganic nanocrystal semiconductors with a dimension of about 2 to 10 nm that contain approximately 100 to 10,000 atoms per individual particle. Because QDs have high electron density in their valence band, these electrons can be excited from the valence band to the conduction band. This excitation is triggered by the absorption of radiation. Relaxation of these excited electrons coincides with the emission of visible light, endowing the QDs with fluorescence activities. QDs are applicable in bioimaging because QDs offer near-infrared emissions that is rare in organic dyes. Since cells can also absorb UV-light and produce background emission leading to poor contrast during bioimaging, near-infrared sensitive materials like QDs are, therefore, a good alternative to explore.²⁹ The optical properties and the electronic properties of QDs depend on the NP composition and size. Due to their high quantum yield and excellent photoluminescence, QDs have been exploited in imaging and as optical sensors such as in cancer research. Some common examples of metals used in producing QDs include; selenium, zinc, tellurium, and cadmium.^{30,31}

Metal-based QDs have undesirable properties making their bio-applications limited. For instance, metal Cd²⁺-based QDs can aggregate to membrane structures such as mitochondrion, and DNA to induce oxidative stress. The Cd²⁺ also binds with sulfhydryl of proteins to cause

severe cytotoxicity. Cadmium-based QDs is also reported to be toxic to vertebrate even at low concentrations.^{29,30,31}

Even though silicon and germanium, belong to the same group in the periodic table as carbon, carbon-based QDs (also called carbon dots) provide a more effective solution in the development of alternative QDs with wide bio-application. This explains why carbon-based QDs has gained much attention in biomedical applications such as bioimaging.^{32,28}

Carbon Dots

Carbon dots (CDs) is carbon base nanomaterials, that can be classified under quantum dots because of its smaller particle sizes, semi-conductivity, zero-dimension, high photostability, tunable emission, and large two-photon excitation cross-sections. CDs have some exceptional properties such as non-blinking fluorescence, high solubility that make their application feasible in bioimaging research. CDs typically have particle diameters between 2nm to 10 nm.^{33, 34} They are very small carbon nanoparticles with comparatively intense fluorescent activity over a wide range of wavelengths.^{35,36,37,38}

Moreover, CDs can be functionalized by various chemical groups on their surface. Most significantly, CDs are more environmentally friendly than other NP-based DDS materials. CDs have been widely used in optical, biological, environmental, and energy-related research as shown in figure 3.^{14, 39} Besides these properties, CDs also have inherent medicinal properties as inhibitors of insulin fibrillation and the suppressors of cancer cells including MCR-7 cancer cells lines and breast cancer cells lines (MDA-MB-231). This observed cancer inhibition is attributed to the formation of a large amounts of reactive oxygen species.^{40,41}

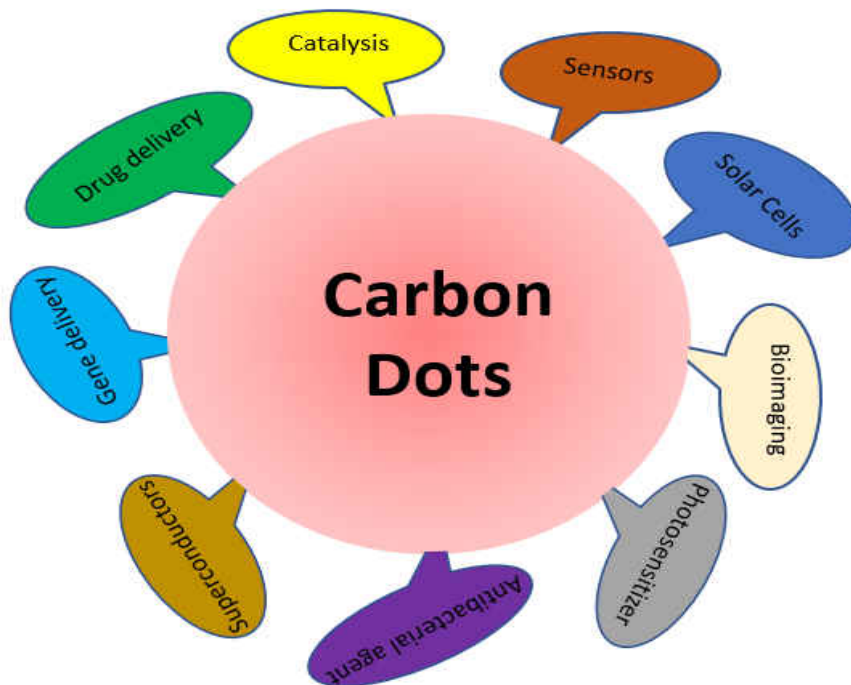


Figure 3. Different applications of Carbon Dots

Carbon Dots as DDS

CDs are among the top candidate in designing new NP-based DDS. With their small sizes, inertness, and excellent water solubility, CDs can easily be absorbed by the kidney in order to pass out via the urine. It is therefore easier to clear the CDs out of the body. That is, the accumulation leading to cytotoxicity is prevented. Functional groups include COOH, OH, and NH₂ on the CDs surface can be further modified for other conjugation. In research where CDs were used as a DDS, doxorubicin (DOX) was successfully conjugated onto CDs with a high drug loading capacity. In the cytotoxicity assay test, the IC₅₀ values were found more effective than the drug alone against the MCF-7 cancer cell line. The CDs-DOX complex was reported to have a lower IC₅₀ compared to the free DOX. This proves that the CDs can be used as a delivery system for anticancer drugs to achieve better anticancer therapy than a standalone anticancer drug.³⁶

Yu Et al. also reported the new folate (L-5-methyltetrahydrofolate) reducible polyethyleneimine CDs (fc-rPEI- CDs) which show visible blue photoluminescence at 360 nm excitation. In their study, the CDs conjugated with the fc-rPEI complex were used as the siRNA gene carrier to deliver the gene into the lung cancer cells. The study indicated that the fc-rPEI – CDs siRNAs complex is selectively accumulated in lung cancer cells via receptor-mediated endocytosis, for effective gene silencing and cancer treatment effect. It was reported that the NP complex still maintains its blue fluorescence even after ten days.³⁵ The integrated theranostic NP complex provides a valuable tool to benefit clinicians in adjusting therapeutic strategy and drug dosage in real-time response by monitoring and tracking the cancer development.⁴²

CDs for Cancer Cell Detection

The use of CDs as an imaging agent has attracted lots of interest in cancer research.^{43,44,45,35} Due to the quantum confinement effect, the nanoscaled CDs inherit special optical properties. As the size of CDs reduces, the electron energy bandgap between the valence and conduction band increases. It leads to several fluorescent colors reflecting the small differences in the CDs size. Other properties such as biocompatibility, easily functionalized surface, and the chemical inertness of CDs make them a good option for bioimaging and bio labeling agent compared to the inorganic quantum dots.^{28 46,47}

For example, Zheng and his coworkers reported that the prepared CDs act as a fluorescence imaging and targeting agent for noninvasive brain cancer glioma diagnosis.⁴⁸ In the report, the fluorescence images showed that the CDs conjugated to aspartic acid (CDs-Asp) had high contrast biodistribution of CD-Asp even after 15 min of intravenous injection. It proved that the prepared CDs-Asp has both bioimaging and glioma cell targeting properties. On the right, a stronger fluorescent signal was observed in the glioma site than that in the normal rat brain. This

also indicated the ability of CDs to freely permeate the blood-brain barrier and detect cancer cells in the brain (glioma cells). That is, CDs-Asp has high selectivity for the brain C6 glioma cells.⁴⁸

Carbon Dots Synthesis

The synthesis of CDs is grouped into two main approaches. They are top-down and bottom-up. A top-down approach in CDs synthesis involved the breakdown of large carbon macromolecules including graphene, nano-diamond, and carbon nanotube to form the CDs. In the latter approach, the CDs is synthesized from the accumulating tiny carbon-containing materials such as ethylene, glycol, and citrates. The top-down approach includes the following method: laser ablation, chemical ablation, and electrochemical synthesis. The bottom-up involve; pyrolysis, hydrothermal, microwave-assisted synthesis.^{49,50} Table 2 is the summary of the various techniques reported on the synthesis of CDs.^{28,51,52}

Table 2. Carbon Dots Synthetic Approach

Method	Size/n m	Quantum Yield (QY)%	Advantages	Disadvantage
Laser ablation	5		Most attainable	Harsh condition and low QY
Electrochemical	6 - 8	4 - 10	Simple	poor control of size
Thermal	2 - 6	0.1 - 8.9	Simple	Low QY
Microwave-assisted	4.5	3 - 21	Simple and less expensive	Poor control of size
Hydrothermal		>50	Simple, highly water-soluble	poor control of size
Template			Colloidal stability	Expensive method

Among all these methods, the hydrothermal treatment also known as solvothermal carbonization is of great interest for our research. This is because, the method is a low-cost, simple, ecofriendly, and non-toxic path to produce CDs. This process involves just one step reaction making it the simplest among all the methods. Depending on the precursor used in the synthesis the fluorescence quantum yield (QY) varies. For example, sulfur-doped CDs from cysteine under the hydrothermal method has a QY of 94.5%.⁵³

Target Agent

One of the common methods to improve the specificity of the drug is by using a target agent. The non-specificity of the many anticancer drugs to the cancer site(s) leads to a low therapeutic effect. When a target agent is attached either directly to the drug or the drug-DDS complex, the conjugate can then specifically bind to its complementary cellular receptor. This

specific binding aided by the target agent help improve the overall cell specificity and increase the drug uptake by the target cells.⁴⁹ This will help reduce the toxic effect of the attached drug on neighboring healthy cells and further minimize the side effects of the administered drug.⁵⁴ The target agents used for cancer identification depend on the type of cancer cell receptor expressed by the cancer cells. The use of a target agent in cancer chemotherapy is reported to enhance the selectivity of cancer drugs.^{55, 29}

The type of receptor on the cancer cell determines which target agent will be used. Ligand-based targeting receptor is by far the most highly used in cancer research. Examples of the ligand-based targeting receptors include; human epidermal growth factor receptor-2 (HER2), epidermal growth factor receptor (EGFR), transferrin receptor (TfR), and prostate-specific membrane antigen (PSMA), carbonic anhydrase IX, biotin receptors, and folate receptor (FR).^{53,54} It is therefore significant to select the best target agent for effective drug therapy. To choose the match target agent for the drug(s), the requirements are that; 1) high affinity of the target agent to the receptor of cancer cells; 2) the receptor should have a high expression on the cancer cell than on healthy cell, for example, folate targets FR which is overexpressed on many cancer cells.^{56,57}

Folic Acid

In this current research, folic acid (FA) is selected as the target agent to help deliver anticancer drugs and as the imaging agents. FA is highly biocompatible, nontoxic, stable, biodegradable, and can be used as a DDs. FA is an essential artificial food additive added to food to supplement folate loss during food processing. FA is essential because it is required in the body to synthesize purine and pyrimidine needed to build and repair nucleotides. FA is water-soluble and has high bioavailability than naturally occurring folate.⁵⁸ FA is reported to target the

folate receptor that is present on many tumor cells. The structure of the FA is represented in figure 4. Human cancers such as breast cancer, lung cancer, and prostate cancer are known to have the alpha Folate Receptor (FR- α) which is overexpressed on their cell surface. The FR- α has a high affinity for folate and it reduced form-folic acid. For instance, HeLa cells are cervical cancer cell line that has overexpressed FR on its cell membrane. When the HeLa cell line was incubated with the FA-CDs complex, it was found that the CDs readily permeated the cancer cells and gave a measurable fluorescence signal. A comparable low level of fluorescence was observed when only CDs are used. In another set-up, when the A549 cell line (cell line with deficient FR on its cell membrane) was used, there was a very low level of fluorescence observed in both the control and FA-CDs complex. It demonstrates that the use of FA can effectively target FR-positive cancer cells.^{53,54}

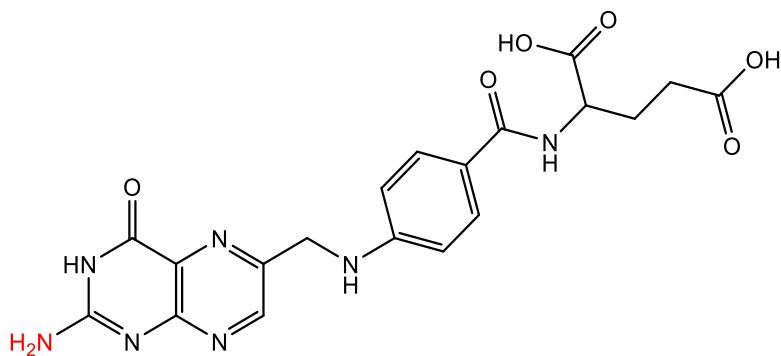


Figure 4. The structure of folic acid

Cocktail Chemotherapy

One of the main drawbacks of cancer chemotherapy is cancer drug resistance, and the struggle to develop novel anticancer drugs. New drug discovery is costly, and it takes about 15 years for a single cancer drug to be approved. The constraint in time and the cost of developing a new anticancer drug can be minimized by exploring cancer combination chemotherapy.⁵⁹

Besides, due to the physiological complexity of cancer tumors, the use of single anticancer drug therapy may not be enough for effective chemotherapy. Therefore, combination chemotherapy also called cocktail anticancer drug might be an effective approach for modern cancer chemotherapy.²⁰

Cocktail or combination chemotherapy involves the simultaneous use of two or more chemotherapeutic agents often with a different mechanism of action to better kill cancer cells. This approach in chemotherapy is gaining momentum in cancer drug-related research. Unlike single-drug chemotherapy where the drug has one signaling pathway, a cocktail anticancer drug can use different cancer cell signaling pathways. That is the use of cocktail drug systems can drastically increase the overall therapeutic efficacy through additive effects, synergistic effects, and potentiation effects.⁶⁰ Since the use of nanosized DDS is documented to help increase the therapeutic effect of a single anticancer drug, loading multiple drugs onto nanosized DDS may increase the effective therapy of the cocktail drug in multiple folds.²⁰

Jack and Zhang²⁰ reported that when DOX and cyclosporin-A were co-loaded on polyalkylcyanoacrylate (CYA) nanoparticles against DOX resistant leukemia cell line, there was about a two-fold increase in the leukemia cell death. Cancer cell apoptosis was dramatically increased when nanoparticle-DOX -CYA was used as compared to standalone DOX. Therefore the use of cocktail anticancer drug and nanosized DDS could be a powerful tool to improve cancer chemotherapy by overcoming anticancer drug resistance.^{20,61}

Doxorubicin (DOX)

Doxorubicin is one of the frequently used anthracycline anticancer drugs sold under the trade name Adriamycin. DOX is one of the commonly prescribed anticancer drugs as first-line chemotherapy in clinics. The precise DOX mechanism of action on cells remains unclear. For

instance, it is reported that DOX increases the free oxygen radicals which cause oxidative stress results, such as DNA damage, senescence, and cell death.⁶² Another reported mechanism is through the destruction of the mitochondrial membrane in the cell leading to cell death.⁶³

DOX is also reported to inhibit the topoisomerase II enzyme, which usually is responsible for DNA opening and supercoiling. The inhibition of this enzyme leads to the cessation of cell proliferation.¹⁸ DOX is a first-line treatment prescribed against various types of cancers such as leukemias, breast cancer, lymphomas, sarcoma, and lung cancer. Like many other cancer drugs, DOX has some drawbacks, such as non-specificity and somatic cellular toxicity. Other side effects associated with DOX include nausea and vomiting, diarrhea, loss of appetite, missed menstrual period, darkening of your skin or nails, weakness, tiredness, and eye redness. Another problem of DOX is its low affinity for nuclei and limited diffusion into cells.^{64,15,45} The several functional groups present on DOX (figure 5), such as -OH and, NH₂, increase the possibility to attach the drug to either DDS or target agent or both.

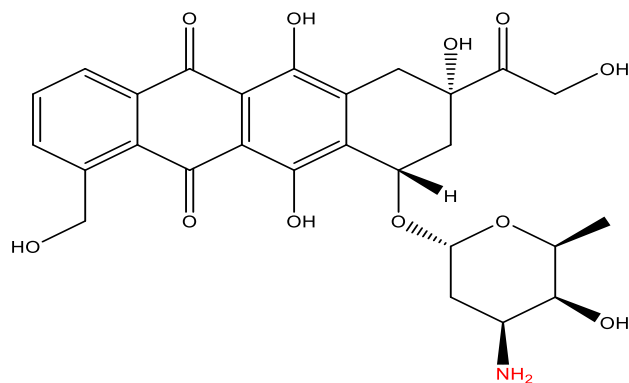


Figure 5. Structure of DOX

Gemcitabine (GEM)

Gemcitabine is one of the first-line anticancer pro-drug commercially known as GEM, which is classified as an antimetabolite.⁶⁵ It is one of the standard cancer drugs administered

intravenously to treat pancreatic cancer. GEM is proven to have a wide spectrum of anticancer activity and can help treat breast cancer, ovarian cancer, non-small lung cancer, and bladder cancer.^{66,67,68,69} The GEM is a deoxycytidine nucleoside analog with two fluorine atoms (figure 6). The presence of the chemical group such as $-NH_2$ and $-OH$ makes it possible to attach this drug to other compounds.

The diphosphate and triphosphate of GEM are reported with anticancer activity.⁶⁵ For instance, GEM-diphosphate is proven to inhibit ribonucleotide reductase (RNR). Ribonucleotide RNR is important in the synthesis of new DNA nucleotides. The triphosphate GEM can competitively incorporate into new DNA as a false nucleotide during cell division. This false nucleotide becomes unrecognizable and irreparable by the DNA repair system. This therefore destructs and terminates DNA chain elongation. This eventually leads to premature cell apoptosis and termination of cell division. GEM is therefore classified as an antimetabolite anticancer drug.

Since GEM targets tissues with high cellular division, it turns to affect other healthy cells that are undergoing regular cell division.^{67,70,69} That is, GEM face a challenge of non-specificity leading to many side effects.⁶⁸ Some common side effects include; joint pain, weakness, numbness diarrhea, dizziness, fever, bone marrow toxicity, and weight loss. Moreover, the hydrophobicity of GEM makes it difficult for the drug to cross the lipid bilayer of cells. This decreases the effective concentration of GEM in the cells.

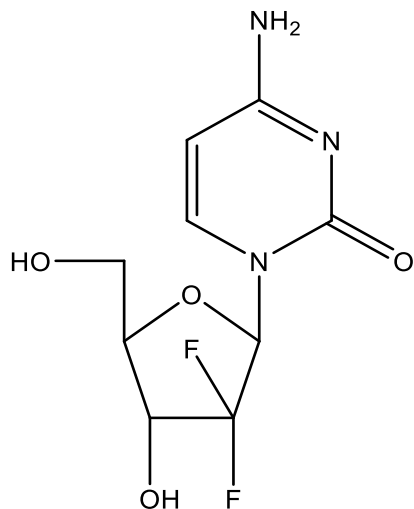


Figure 6. Structure of GEM

Research Plan

The primary goal of this study is to prepare novel CDs based nanoparticles as potential theragnostic for cancer treatment. The NPs complex will comprise of CDs, folic acid (FA) as the target agent, and anti-cancer drug DOX or GEM. Previous work in my research group successfully synthesizes and characterized two series of carbon dots from citric acid and ethylenediamine. DOX was successfully attached to the two series of carbon dot-folic acid complexes via non-covalent linkage. The CDs-DOX and FA-CDs-DOX were also characterized. It was found that the CDs series B (with 1:1 citric acid to ethylenediamine) gave better fluorescence and had higher drug content. However, information on drug load content, drug load efficiency, and the NPs toxicity of these complexes from covalent synthesis is limited and is, therefore, the main aim of this current research. Four primary objectives form the basis of this work.

1. Changing the ratio of CDs to DOX to find the best ratio to give a high drug profile (drug load content and efficiency) by using noncovalent synthesis, and to determine the pH-dependent DOX releases.

2. New series of carbon dots/drug-folic acid complex by exploiting the EDC carbodiimide coupling reaction to form covalent bonding. The anticancer drugs DOX, and GEM will be compared. The drug load efficiency and drug load content will also be determined. The complexes synthesized will be characterized by UV-vis, FTIR for functional groups, and fluorescence.
3. All the prepared FA-CDs- drug complex via covalent/noncovalent bonding will be tested on cancer cell lines to assess parameters such as cell viability, and IC_{50} .
4. Loading both DOX and GEM on the CDs and further characterization.

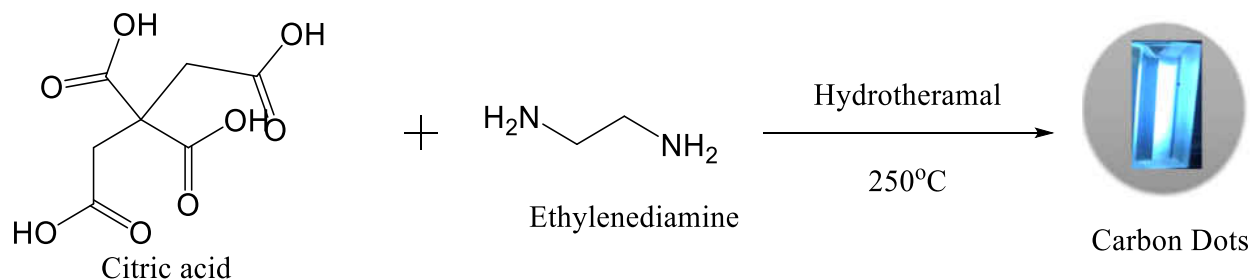
CHAPTER 2. EXPERIMENTAL

General Material

Ethylenediamine, citric acid, Gemcitabine hydrochloride (GEM.HCl), Doxorubicin hydrochloride (DOX.HCl) was purchased from Oakwood Chemicals, two types of dialysis tubes with pore size with molecular weight cut-off of 1.0 KDa and 3.5 KDa, 3-(3-Dimethylaminopropyl)-1-ethyl-carbodiimide (EDC), N-Hydroxy-succinimide (NHS), folic acid (FA), gibco phosphate-buffered Saline (PBS), pH 7.4 (1X) purchased from Fischer scientific.

Synthesis of CDs

In a general method of CDs synthesis, 1.051g (10.41 mmol) of citric acid was dissolved in 335.0 μ L (0.9540 mmol, the ratio is 1:1.1) of ethylenediamine in 10 mL D.I water. The solution was then autoclaved in a Teflon-lined hydrothermal autoclave at 250 °C for 5 hours. To maintain the CDs size consistency, the cooled brown solution was dialyzed using a dialysis bag with a 3.5 KDa cutoff against 500 mL D.I. water for 6 hours. It was then freeze-dried to obtain a brown powered sample. This method was followed as reported by Schneider Et al.⁷¹ and Zhu Et al.³³ with slight modification.



Scheme 1. Hydrothermal synthesis of CDs. The insert picture for CDs showed a brilliant blue solution under UV light

Synthesis of Non-covalent CDs-DOX from DOX.HCl

In a general method, 4.00 mg of the CDs was dissolved into 1.00 mL DI water. This solution was sonicated for 15 minutes. To this solution, 1.00 mL of 0.4 mg/mL DOX.HCl (6.89×10^{-4} mmol/mL, the weight ratio of 1:10) was added and 2.00 mL of 1 X PBS was added to the final mixture. This mixture was then transferred into a 20 mL round-bottomed flask and covered with aluminum foil to prevent photo-degradation. The mixture was stirred at room temperature for 24 hours. The volume of the solution after synthesis was 3.9 mL. 0.2 mL of solution was diluted into 1 mL aqueous solution with D.I water for UV-analysis. The rest of the CDs-DOX was dialyzed with a 1 KDa dialysis tube against 500 mL D.I. to obtain 3.7 mL of solution. From this solution, 0.2 mL was diluted into 1 mL aqueous solution with 1 mL D.I water for UV-analysis. CDs-DOX was prepared by a slight modification of the procedure by Yuan Et.al.¹⁵

Synthesis of Non-covalent FA-CDs-DOX from DOX.HCl

In a general method described by Yuan Et al.¹⁵, 1.50 mL of FA-CDs (8 mg/mL) was first sonicated for 15 minutes, and then 1.50 mL of 0.4 mg/mL DOX.HCl ($1.0345 \mu\text{mol}$) was added. The solution was kept under a stirring condition of 200 rpm at 25 °C in the dark (to prevent photo-degradation of DOX) for 24 hours. The volume of the solution was 3.9 mL. 0.2 mL of the solution was diluted into 1 mL aqueous solution for UV-vis analysis. The rest of the 3.7 mL FA-CDs-DOX solution was dialyzed in a 3.5 KDa dialysis tube against 500 mL D.I water for two (2) hours to obtain a 3.8 mL final product. The volume of the FA-CDs-DOX solution after dialysis was 3.8 mL.

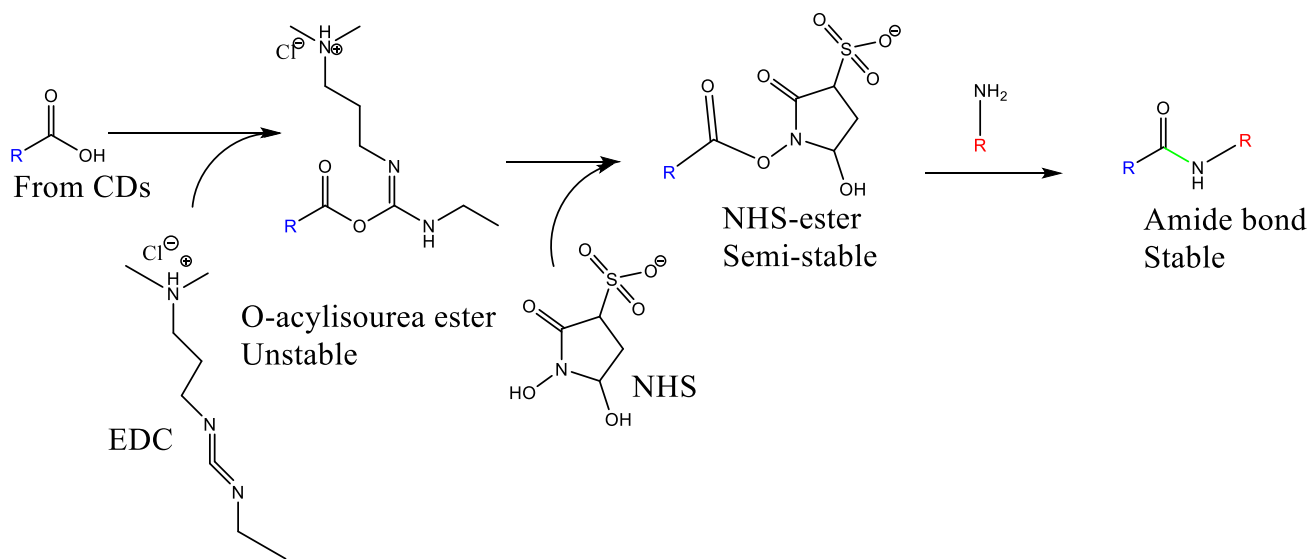
Synthesis of Covalent CDs-DOX or CDs-GEM from DOX.HCl or GEM.HCl

In a general procedure, the prepared CDs (4 mg) was dissolved in 1.5 mL phosphate-buffered solution (PBS, pH 7.4) and sonicated for 15 minutes. To this solution, 0.5 ml of 17mg/ml 1-ethyl-3-(3-dimethylamino propyl) carbodiimide hydrochloric acid (44.3 μ Mol EDC.HCl) was added and stirred for 30 minutes. Then, 0.5 ml of 10.2 mg/ml N-hydroxy succinimide (44.3 μ Mol NHS) was also added and stirred for another 30 minutes. The ratio of the EDC to NHS was maintained at 1:1 in the synthesis. After that, 0.5 ml of 5 mg/ml (8.3 μ Mol) DOX.HCl was added and stirred overnight in the dark to prevent the photodegradation of the DOX.HCl. The overall ratio of the DOX to EDC or NHS was 1:5.3. The final solution was dialyzed against 1 L of D.I water with a 3.5 kDa dialysis tube. The dialysis was carried out for 4 days with the dialysate medium changed every 24 hours. The final solution was lyophilized to obtain brownish solid CDs-DOX⁷² for FTIR analysis. The process was repeated with GEM with a molar equivalent to DOX. That is, 0.5 ml 5mg/ml (8.3 μ Mol) of the GEM was added in replace of the DOX to synthesize the covalent CDs-GEM. All molar ratios were maintained.

Synthesis of Covalent FA-CDs-DOX or FA-CDs-GEM From DOX.HCl or GEM.HCl

In this procedure, CDs (4 mg) was dissolved in a 1.5 mL phosphate-buffered solution (PBS, pH 7.4) and sonicated for 15 minutes. To this solution, 0.5 ml 17 mg/ml 1-ethyl-3-(3-dimethylamino propyl) carbodiimide hydrochloric acid (44.3 μ Mol EDC.HCl) was added and stirred for 30 minutes. Then, 0.5 ml of 10.2 mg/ml N-hydroxy succinimide (44.3 μ Mol NHS) was also added and stirred for another 30 minutes. The ratio of the EDC to NHS was kept at 1:1 in the synthesis. Next, 0.5 ml of 5 mg/ml (8.3 μ Mol) DOX.HCl was added and stirred overnight in the dark to prevent the breakdown of the DOX.HCl by light (DOX.HCl is photosensitive). To this solution, 0.13 ml of 0.1 mg/ml folic acid (FA) was added and stirred overnight in the dark.

The ratio of the DOX to the FA was 280:1. The final solution was dialyzed against 1.0 L of D.I water with a 3.5 KDa size cutoff point for 4 days. The dialysis medium was changed every 24 hours to ensure complete removal of unreacted CDs, NHS, EDC, and DOX. The dialysis setup was kept in the dark to prevent the breakdown of DOX. UV-vis analysis was done before and after dialysis. The final solution was lyophilized to obtain brownish solid FA-CDs-DOX for FTIR analysis. The process was repeated with GEM with a molar equivalent to DOX. That is, 0.5 ml 5mg/ml (8.3 μ Mol) of the GEM was added in replace of the DOX to synthesize the covalent CDs-GEM. All molar ratios were maintained. This procedure was followed with a small modification to the method documented by Liyanage at al.⁷²



Scheme 2.EDC/NHS coupling reaction

Spectroscopy

The UV-vis properties of the absorption of the samples and intermediates were recorded with PharmaSpec UV-1700 PerkinElmer ultraviolet-visible UV-vis spectrophotometer in a 1 cm quartz cuvette. 0.01mg/ml of the solution was prepared and scanned from 190 nm to 600 nm to capture all peaks present in the samples and intermediates.

The fluorescence emission spectra measurements were taken with the FluoroMax-3 spectrophotometer. About 1.5 ml of the aqueous solution of the nanoparticle was transferred into a 1cm quartz cuvette for analysis. In the fluorescence analysis, excitation-dependency properties of the samples were determined by exciting the sample with a different wavelength from 300 nm to 390 nm (Monochromators having Xenon arc lamp) with 10nm increment. All samples were scanned from 400 nm to 700 nm with a 10 nm increment.

The functional groups present on the nanoparticles were recorded using a Shimadzu IRPrestige FTIR with ATR accessory. The solid nanoparticle after lyophilization was scanned from 4000 cm^{-1} to 450 cm^{-1} .

CHAPTER 3. RESULTS AND DISCUSSION

Synthesis of CDs

In this research, the synthesis of CDs was done using a single-step hydrothermal treatment of citric acid and ethylenediamine. Citric acid is an important compound that is commonly found in food and food supplements.⁷³ In the synthesis of the CDs, citric acid represents the carbon source and ethylenediamine as the nitrogen source. Ethylenediamine is also commonly used as a surfactant to enhance the bioactivity of drugs such as aminophylline.⁷⁴ During the synthesis, the preferred molar concentration ratio of citric acid to ethylenediamine was kept at 1:1.1. In previous studies, this ratio had a better and consistent drug loading profile according to the previous work done by Dada.⁷⁵ Also, as Zhu Et al.³³ reported, CDs produced from this ratio is easy for TEM imaging because this ratio produces CDs with uniform dispersion without any apparent aggregation of the NPs. The CDs solution was dark brown which according to Pandey Et al.⁷⁶ indicated the presence of CDs. The dialysis of the CDs solution ensures consistency in the CDs NPs size and produces CDs devoid of any by-products on its surface. After the purification and subsequent lyophilization, the CDs yield was approximately 30 %. This low yield might be a result of the loss of CDs during the dialysis procedure. The particle size of the CDs was around 3-5 nm determined by dynamic light scattering, DLS.

Covalent Synthesis of CDs-DOX/CDs-GEM Complexes

The covalent synthesis of the CDs-DOX/CDs-GEM complex was completed using the EDC/NHS coupling reaction reported by Liyanage Et al. with slight modification.⁷² The carboxylic group on the surface of the CDs was conjugated with the amino group in the DOX/GEM. This coupling reaction allows for the formation of a non-cleavable amide bond

between the CDs and DOX/GEM. In the procedure, the EDC activates the carboxylic acid groups on the CDs to form the O-acylisourea intermediate. The O-acylisourea intermediate is often unstable in an aqueous medium and is therefore stabilized by the NHS to allow for nucleophilic attack by the amino groups on DOX/GEM to form the amide bond by displacing the EDC as shown in scheme 2.⁷⁷ The unreacted reagents were washed off via dialysis to obtain the CDs-DOX/GEM complex. The quantity of DOX was calculated using the λ_{max} of DOX at 485 nm referring to the UV-vis standard calibration curve (figure 7) where various concentrations of DOX solutions were plotted against absorbance. While in the case of the GEM complex, the concentration of the bonded GEM at λ_{max} of 269 nm was calculated from the GEM standard curve (figure 8).

Synthesis Covalent of FA-CDs-DOX / FA-CDs-GEM Complexes

The covalent synthesis of the FA-CDs-DOX/FA-CDs-GEM complex was completed using EDC/NHS coupling reaction.⁷² The carboxylic group on the CDs surface was conjugated with the amino group in the DOX/GEM. To this solution, the folic acid was electrostatically added to form the covalent FA-CDs-DOX/ FA-CDs-GEM complex. The unreacted reagents such as free DOX/GEM, CDs, FA, EDC, and the NHS were washed off via dialysis to obtain the covalent FA-CDs-DOX/ FA-CDs-GEM complex. The average diameter of covalent FA-CDs-DOX is 1.74 nm, which is smaller than the FA-CDs-GEM complex. For the FA-CDs-GEM, the quantity of the bonded GEM at λ_{max} of 269 nm was calculated from the GEM calibration curve. The average diameter of covalent FA-CDs-GEM is 3.57 nm.

Calibration Curve for DOX

The concentrations of DOX present in DOX NPs complexes were determined using the standard calibration curve in figure 7. Different concentrations of DOX were prepared and the UV

absorbance of the DOX for each serial concentration was recorded at 485 nm. DOX standard graph was plotted with concentration against absorbance. The unknown concentration of the DOX from each complex produced was calculated from the DOX standard plot equation given by $y = 20.676x - 0.0237$.

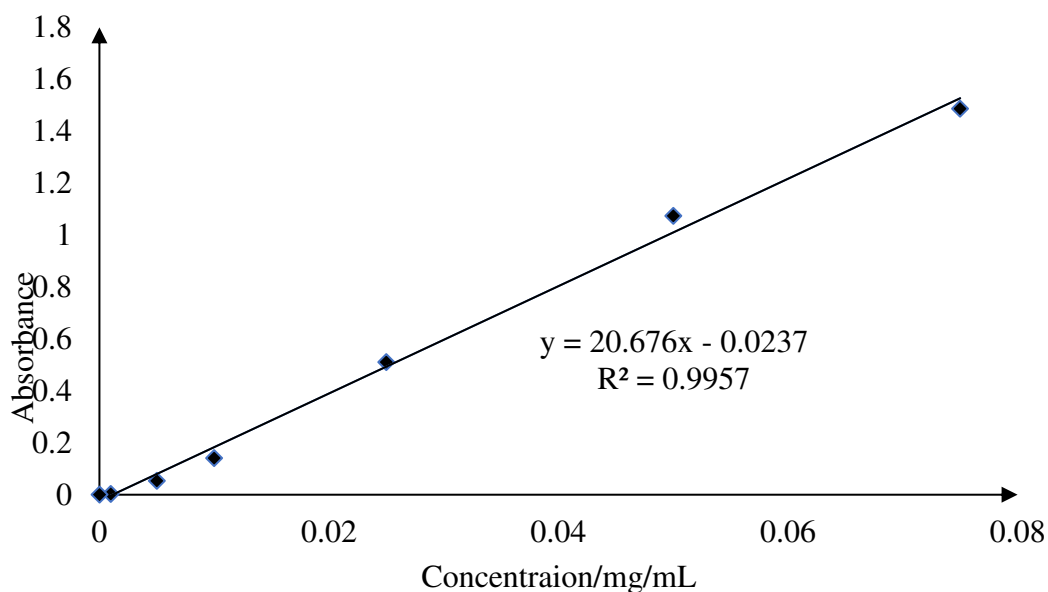


Figure 7. Calibration curve of pure DOX

Calibration Curve for GEM

The concentrations of GEM present in the complexes were determined using the standard calibration curve in figure 8. Different concentrations of GEM.HCl was prepared in DI water. The absorbance of the different concentrations of the GEM at a maximum peak of 269 nm was taken and plotted against the concentration to obtain the standard calibration curve.^{78,79}

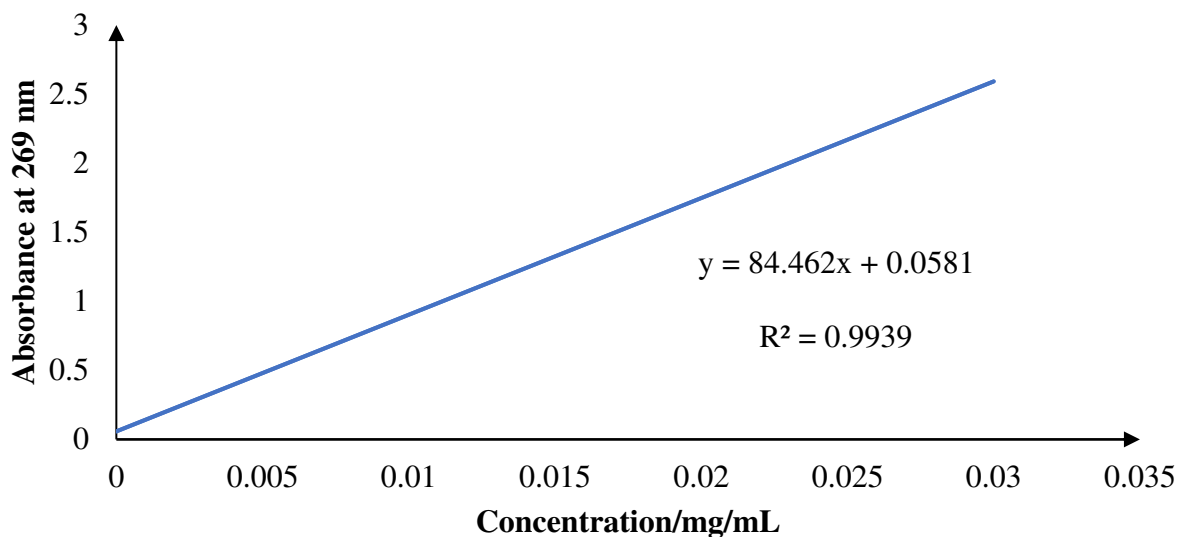


Figure 8. Standard curve of GEM.HCl showing concentration (in mg/mL) against absorbance at 269 nm

Drug Load Content (DLC) and Drug Load Efficiency (DLE)

In a general procedure, DLC and DLE were determined using the method as described by Gao Et al.⁸⁰ with slight modifications. After the synthesis of the complex, the unbounded drug was determined to calculate the DLE and DLC. 0.2 ml of the complex after the synthesis was diluted with 5 ml D.I water for UV-vis analysis. The maximum UV absorption peak of the unbounded DOX at 485 nm was recorded. For the GEM, the absorbance of the free GEM at 269 nm was also recorded. The corresponding concentration of the free drug using their respective linear equation. The difference between the free drug and the initial amount of the drug was determined. This difference corresponds to the amount of the drug in conjugation. The DLC and DLE were then calculated using equation 1 and 2 respectively.³⁷ The drug load profile for the complexes is summarized in table 3.

$$DLC (\%) = \frac{\text{amount of drug in conjugation}}{\text{initial amount of the CDs}} \times 100\% \quad \text{Equation 1}$$

$$DLE (\%) = \frac{\text{amount of drug in conjugation}}{\text{initial amount of the Dox}} \times 100\% \quad \text{Equation 2}$$

Table 3. Drug Load Profile for Covalent and Noncovalent Complexes

NPs	Covalent		Noncovalent	
	DLE%	DLC%	DLE%	DLC%
FA-CDs-DOX	71	80	83.8	3.9
CDs-DOX	53.7	60.9	75	7.03
FA-CDs-GEM	69.6	37.8		
CDs-GEM	75.1	46.9		

UV-vis Analysis of Nanoparticles

The most common optical characterization study of CDs is UV-vis analysis. The CDs solution was scanned in a broad wavelength from 900 nm to 190 nm in the UV-vis analysis. The CDs displayed strong and distinct absorption peaks from 200 nm to 400 nm specifically at 198 nm, 240 nm, and 344 nm as shown in figure 9. These peaks are consistent with literature data.^{4,3,37} The peak at 198 nm represents $\pi \rightarrow \pi^*$ electron transition in C=C bonds while that of 240 nm peak is $n \rightarrow \pi^*$ electron transition. Also, the peak at 344 nm is attributed to the C=O and C-N bonds with electron transition at $n \rightarrow \pi^*$ transition in sp^2 hybridization of carbonyl groups on CDs surface.^{37,34,81,64,33}

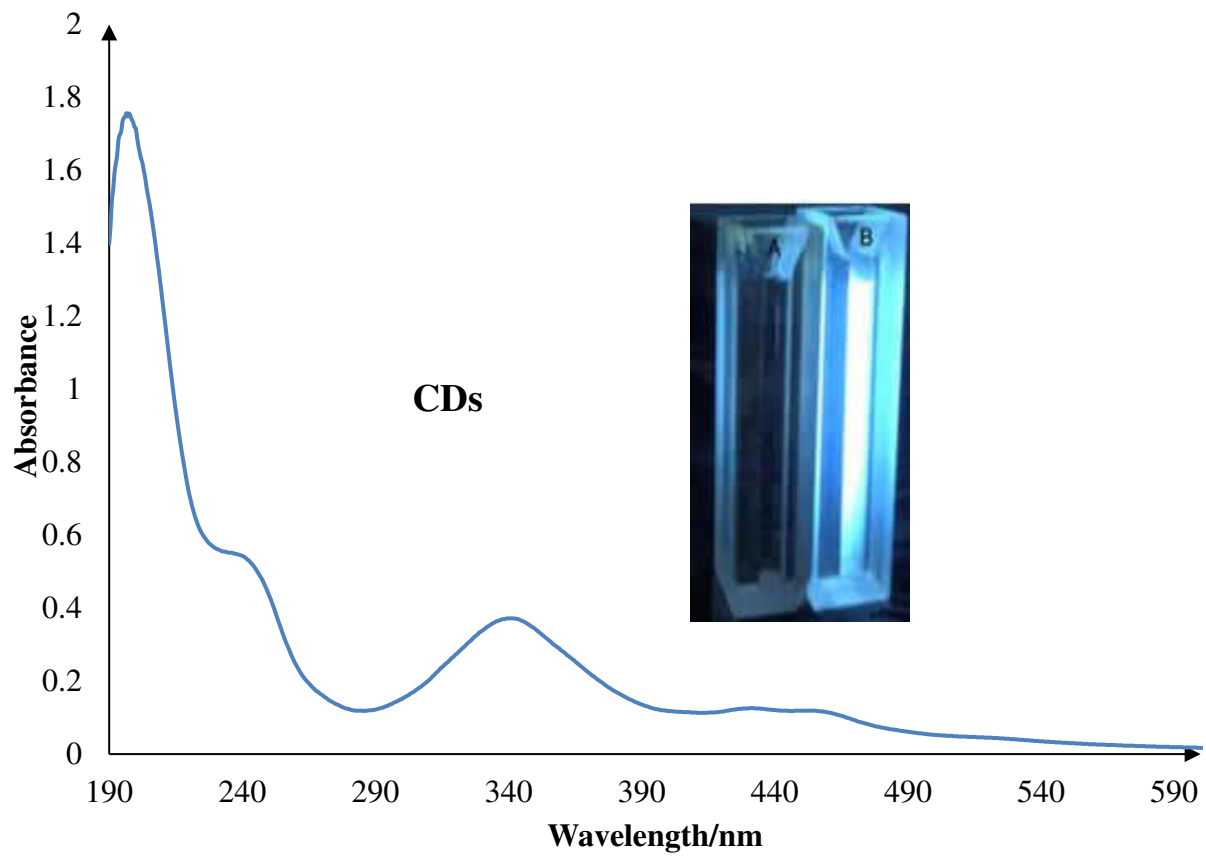


Figure 9. UV-vis of 0.01mg/ml CDs showing the peaks 198 nm, 240 nm, and 344 nm.

The insert is a photograph of water (A) and CDs (B) under handheld UV-light.

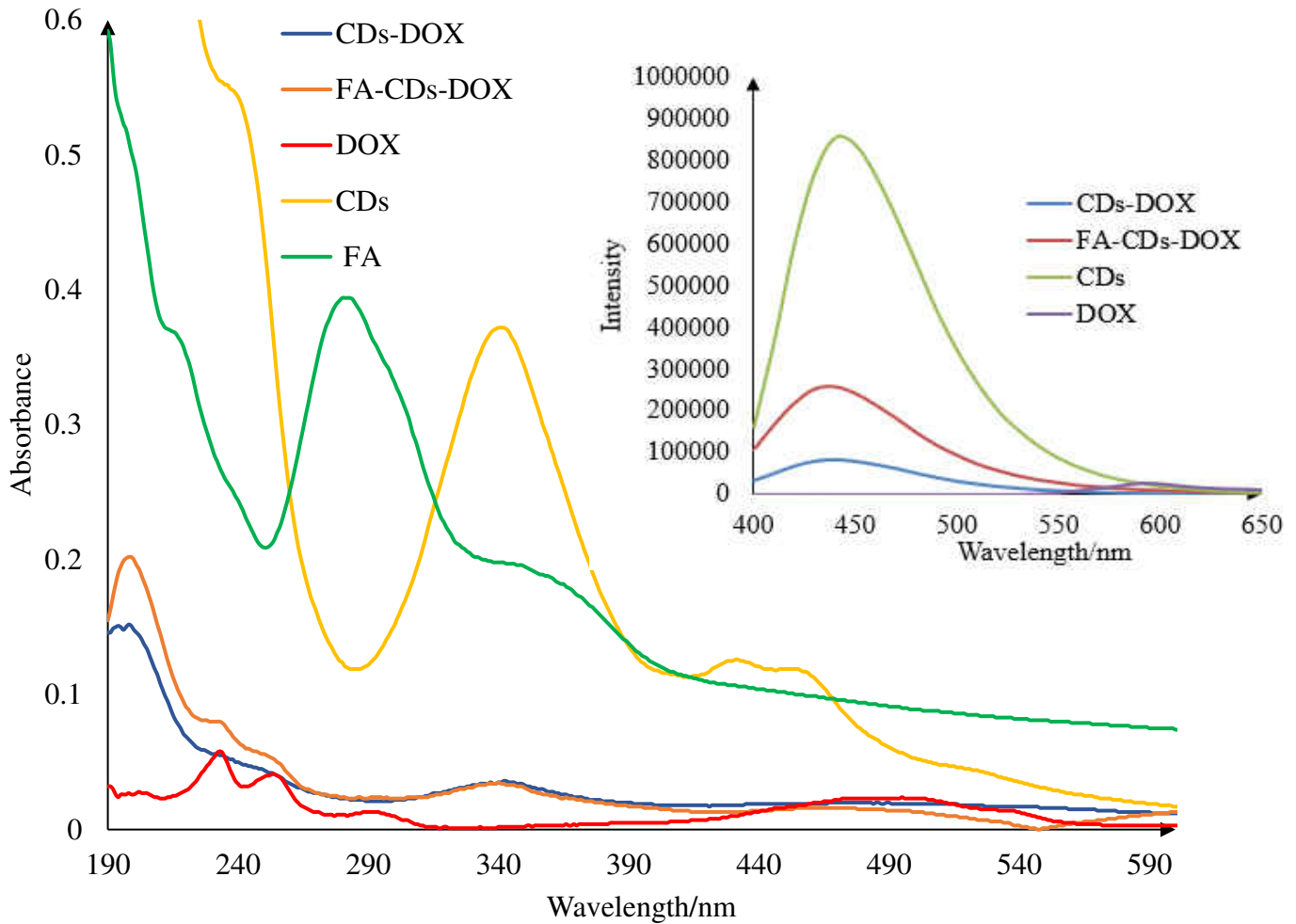


Figure 10. UV-vis of 0.01 mg/ml CDs-DOX, FA-CDs-DOX, and DOX.

The insert shows fluorescence spectra of the pure CDs, DOX, CDs-DOX, and FA-CDs-DOX excited at 360 nm

The covalent FA-CDs-DOX and CDs-DOX complexes in figure 10 exhibited the main UV-vis absorption peaks of CDs and DOX. In the covalent FA-CDs-DOX, the characteristic peaks are at 201 nm, 235 nm, and 340 nm. Among them, there is a blue shift from 198 nm to 201 nm, and a redshift from 240 nm to 235 nm. Similar characteristic peak shifts can be observed in the covalent CDs-DOX. In both complexes, the bonded DOX peak at 480 nm indicates a redshift

relative to the pure DOX at 485 nm. The pure FA has an absorption peak at 285nm. From the FA-CDs-DOX, there is a peak at 255 nm. This peak could be a combinational peak from the attached FA since this peak cannot be observed in the CDs-DOX. The Uv-vis spectra of the covalent FA-CDs-DOX and CDs-DOX confirm the successful fabrication of the complexes.

82,37,81

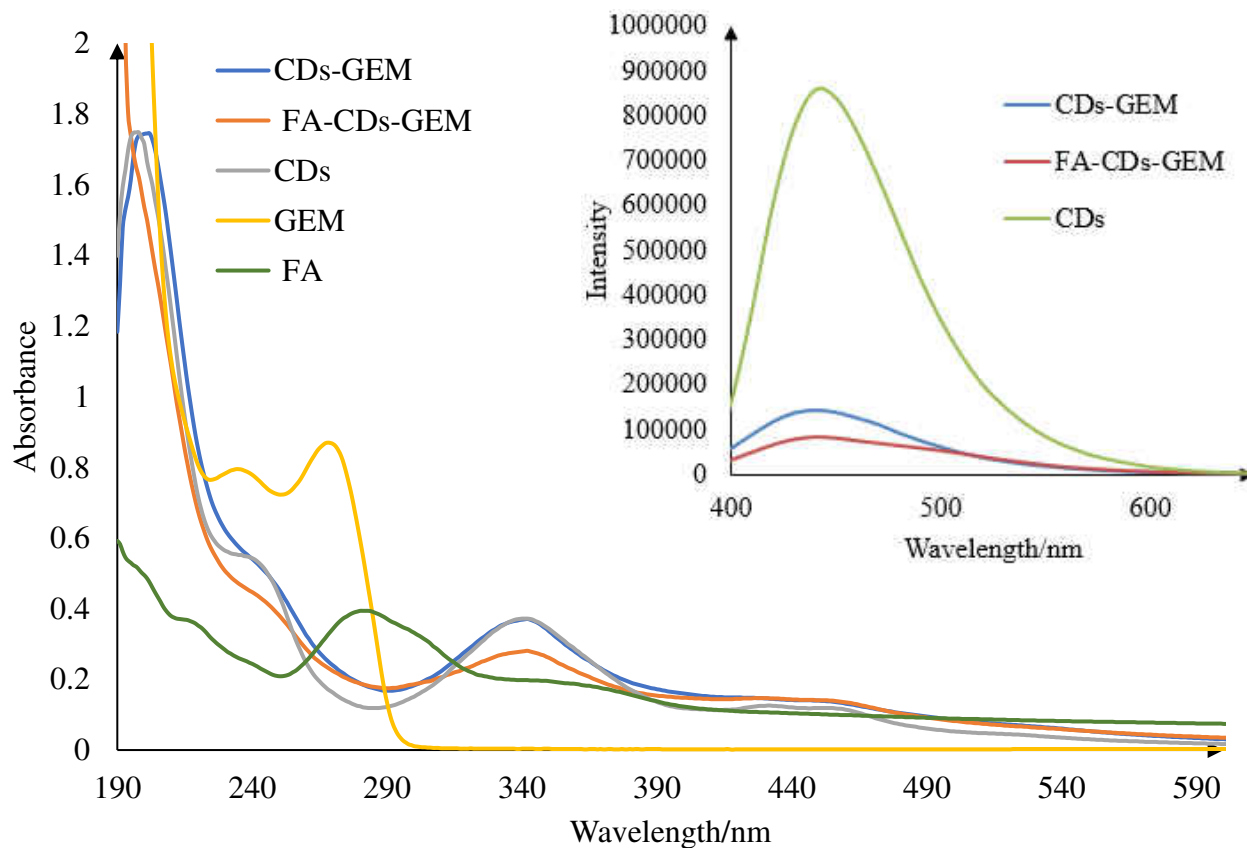


Figure 11. UV-vis spectra of obtained CDs (0.01mg/ml), CDs-GEM (0.01mg/ml), and 0.01mg/ml FA-CDs-GEM complex. The insert shows fluorescence spectra of CDs, CDs-GEM and FA-CDs-GEM excited at 360 nm.

The FA-CDs-GEM and the CDs-GEM covalent complexes maintained the two UV-vis absorption peaks of the attached CDs at 240 nm and 344 nm as seen in figure 11. In the CD-GEM complex, there is a blue shift of characteristic CDs peak from 198 nm to 204 nm. Also, the peak at 240 nm is the blue shift of one of GEM's typical peaks at 236 nm. A typical pure FA peak occurs at 285nm. In the FA-CDs-GEM, there is a small peak at 250nm which can be observed when zoomed out. This peak is absent in the CDs-GEM. Therefore, this peak might be a blue shift peak of the FA confirming the successful formation of the FA-bound complex. The presence of the absorption peaks 204 nm, 240 nm, and 344 nm for CDs, and the absorption peak of the GEM at 269 nm on the complex shows successful fabrication.

Photoluminescence Analysis of Nanoparticle

Another optical property of the nanoparticles that is vital to their application in biological research, specifically in bioimaging is photoluminescence (PL). The PL characteristic of CDs solution was observed at different excitation wavelengths from 300 nm to 390 nm, with 10 nm increment as seen in figure 12. The PL spectra of the CDs presented an excitation-dependent emission behavior. The PL intensity increased progressively from excitation of 320 nm to 360 nm and started to decrease beyond the excitation at 360 nm. This excitation-dependent PL property exhibited by the CDs solution is useful in multicolor biological imaging.^{36,82} Concerning the fluorescence spectra, the maximum excitation, and emission wavelengths were respectively found at 360 and 450 nm as already reported.^{36,33} The UV-vis properties and the fluorescent behavior of CDs are attributed to the electronic surface band structure which also affects the energy bandgap of the CDs.

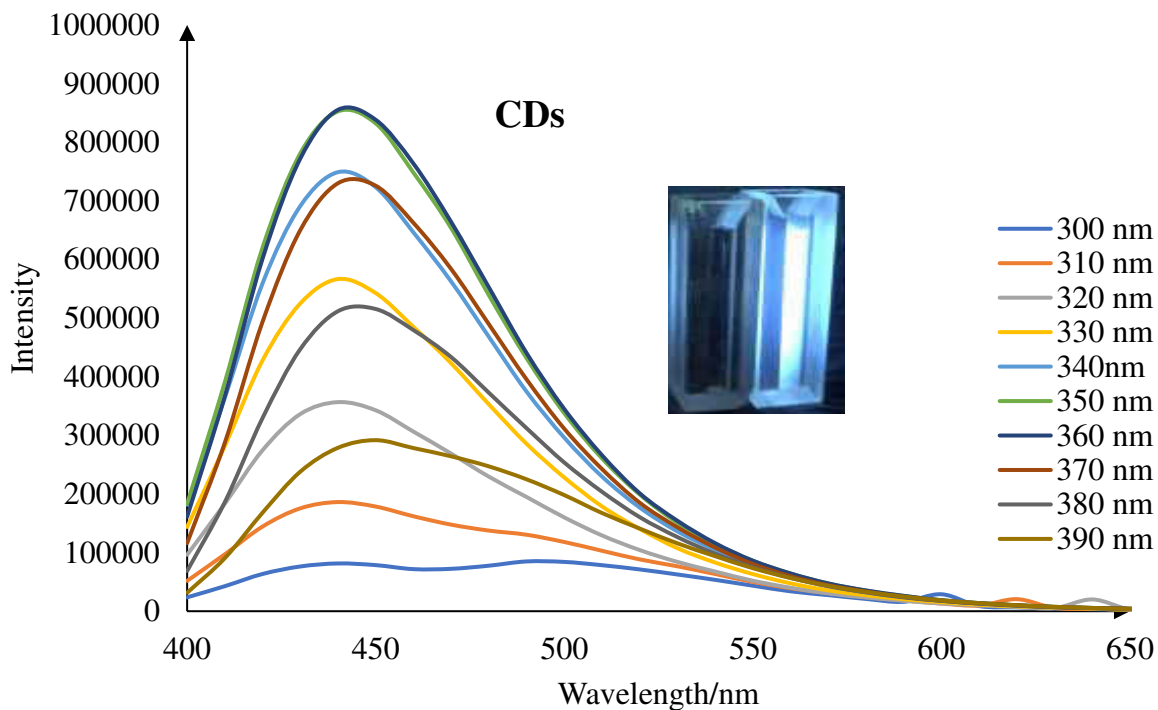


Figure 12. FL spectra of CDs (0.01 mg/mL). The inset at the upper-right corner shows a photograph of D.I water (left), and CDs in an aqueous solution (right) under visible light

In Figure 13A and 13B respectively for CDs-DOX and FA-CDs-DOX, both NPs exhibited distinct emission peak at 450 nm ($\lambda_{ex}=360$ nm) as CDs. Compared the emission peak intensity, the trend is CDs > FA-CDs-DOX > CDs-DOX. According to Hong Et al.³⁶, the decrease of the emission intensity might be as a result of the attached DOX. That is, the DOX might have slightly quenched the CDs emission. The drop in the intensity might indicate successful fabrication of DOX to the CDs.³⁶ Moreover, the blue color of the CDs-DOX is much brighter than the solution of FA-CDs-GEM. this difference in the emission might be due to the presence of the FA. This and the decrease in the emission intensity in the FA-CDs-DOX complex might be contributed by the attached FA.

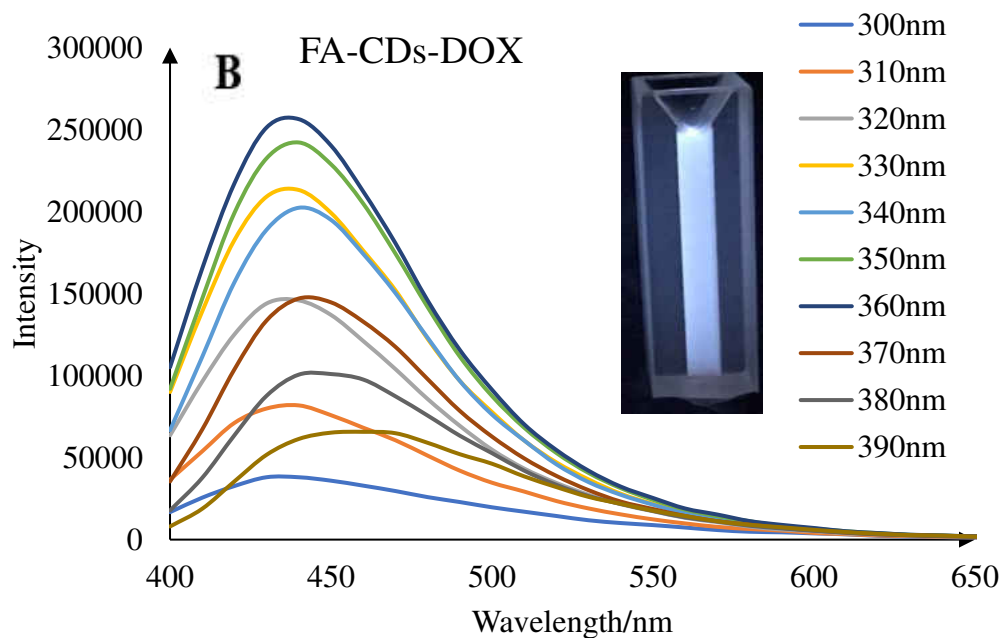
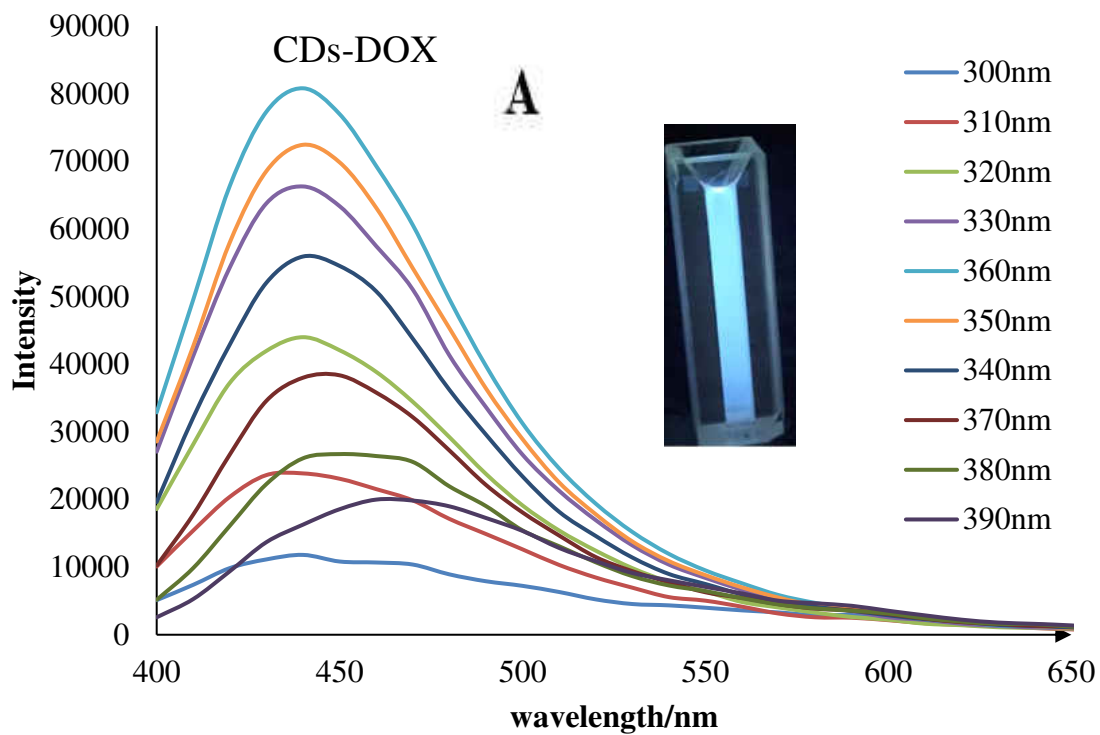


Figure 13. FL spectra of 0.01mg/mL covalent DOX complexes

CDs – DOX (A) and 0.01 mg/mL FA – CDs – DOX (B) at different excitation wavelength (300 nm – 390 nm). The insert photograph is the solution of the complex under UV light.

Similar fluorescent behavior was observed in the NPs with anticancer drug GEM as seen in figure 14A and 14B. That is, the emission intensity increased gradually from excitation of 320 nm to 360 nm and started decreasing after 360 nm. Again, the highest emission intensity occurred at 450 nm when excited at 360 nm. These trends are similar to the fluorescence behavior of the CDs. For the FA-CDs-GEM complex, when it was excited at 310 nm, 390 nm, 380 nm, the emission intensity shifted to around 500 nm is presented in figure 14B. This change explains why the FA-CDs-GEM complex appears greenish under UV light. This shift is observed as an emission redshift. A similar observation was seen in the CDs-GEM when it was excited at 380 nm and 390 nm. This phenomenon was also reported by Liyange Et al.⁷² This redshift is a result of the differences in energy levels associated with the various surface states formed by distinct chemical groups on the FA-CDs-GEM and the CDs-GEM surface.^{83,71} However, the CDs-GEM solution under UV light shows a similar color as the pure CDs. The difference in the color of the FA-CDs-GEM and the CDs-GEM might be as a result of the FA bounded to the complex. The redshift, difference in solution color, and the reduction in peak intensity in both FA-CDs-GEM and CDs-GEM could further confirm the successful formation of GEM complexes.^{15,36,41}

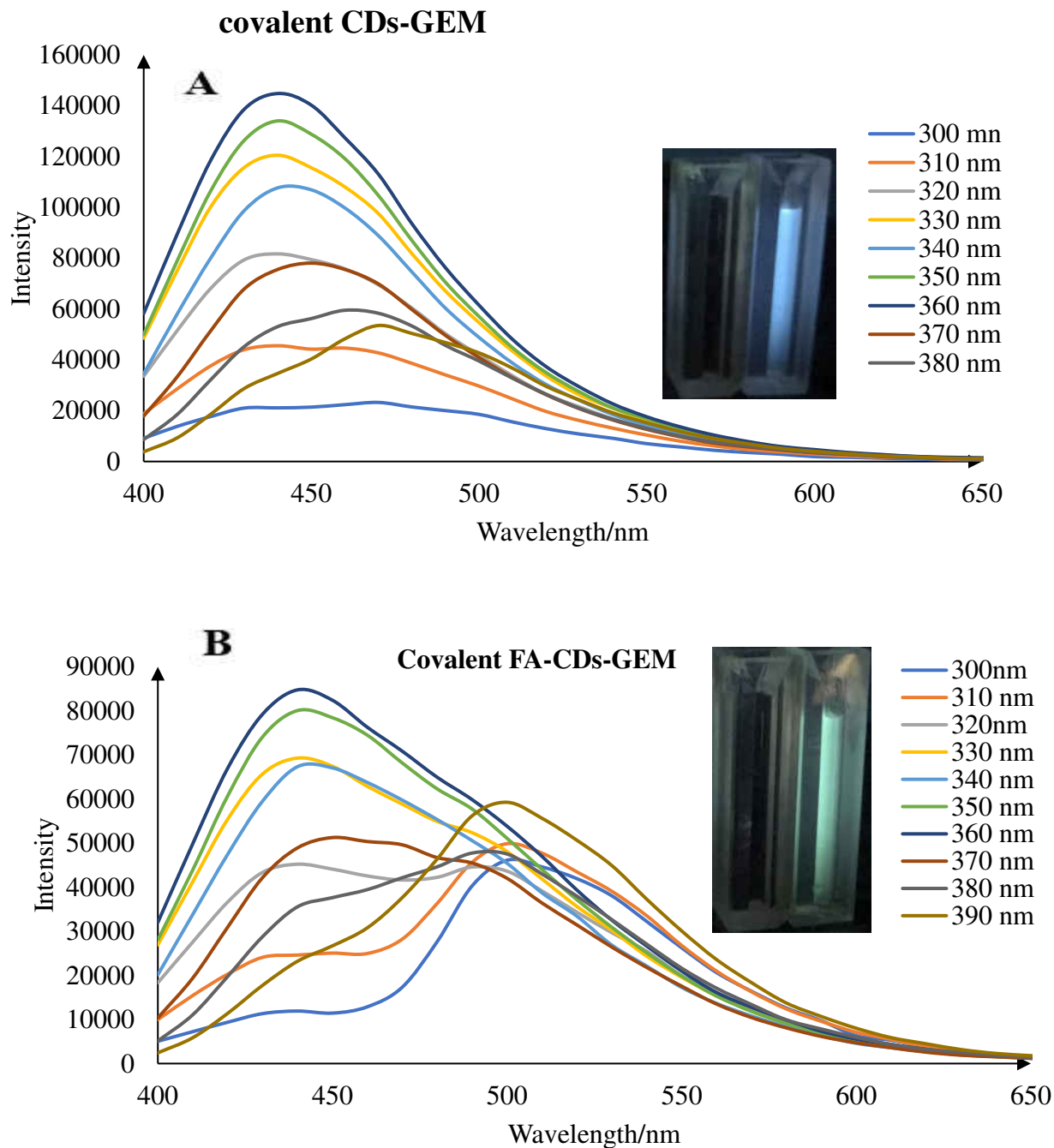


Figure 14. FL spectra of 0.01mg/mL covalent GEM complexes.

CDs-GEM (A) and 0.01 mg/mL of FA-CDs-GEM (B) excited from 300 nm – 390 nm. The inset at the upper-right corner shows a photograph of CDs-GEM (A) and FA-CDs-GEM (B) in an aqueous solution (right) and D.I water (left) under visible light.

FTIR for Nanoparticle

The chemical groups present on the surface of the NPs were determined by FTIR. The FTIR spectrum for CDs in figure 15 shows predominant peaks occurring at 3228 cm^{-1} , 1651 cm^{-1} , 1539 cm^{-1} and 1045 cm^{-1} . The absorption bands at 3228.8 cm^{-1} corresponded to O-H stretching vibrations in carboxylic acid or N-H stretch vibration in primary NH_2 . The N-H bending vibration is observed around 1651 cm^{-1} , which is overlaid by the peaks of the carbonyl functional group (C=O) on the CDs surface.⁷¹ The bands appearing at 1045 cm^{-1} can be assigned to C-O-C in stretching bond. The absorption peaks suggest the presence of carboxylic acid, hydroxyl groups, and amine functional groups. These characteristic peaks of the CDs are consistent with reports by Yuan Et al.⁸² These functional groups contribute to the high-water solubility of CDs.

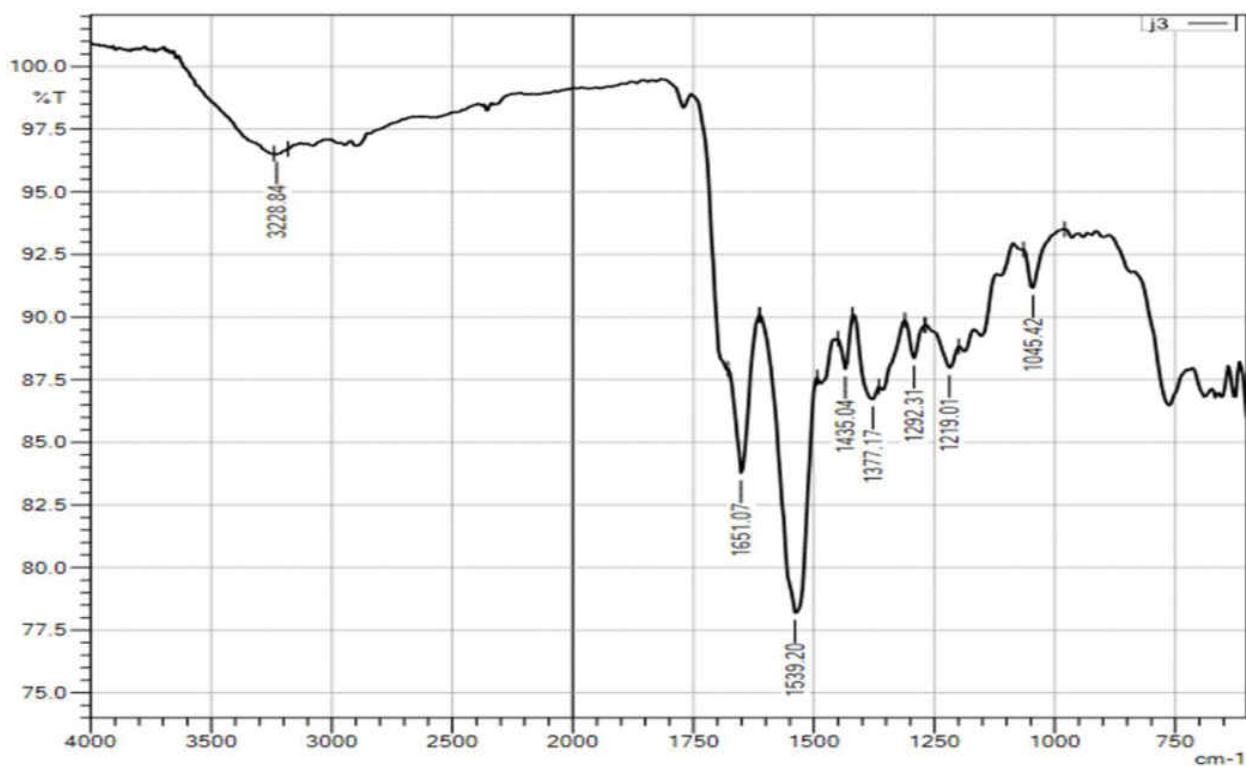


Figure 15. ATR-FTIR spectra of CDs

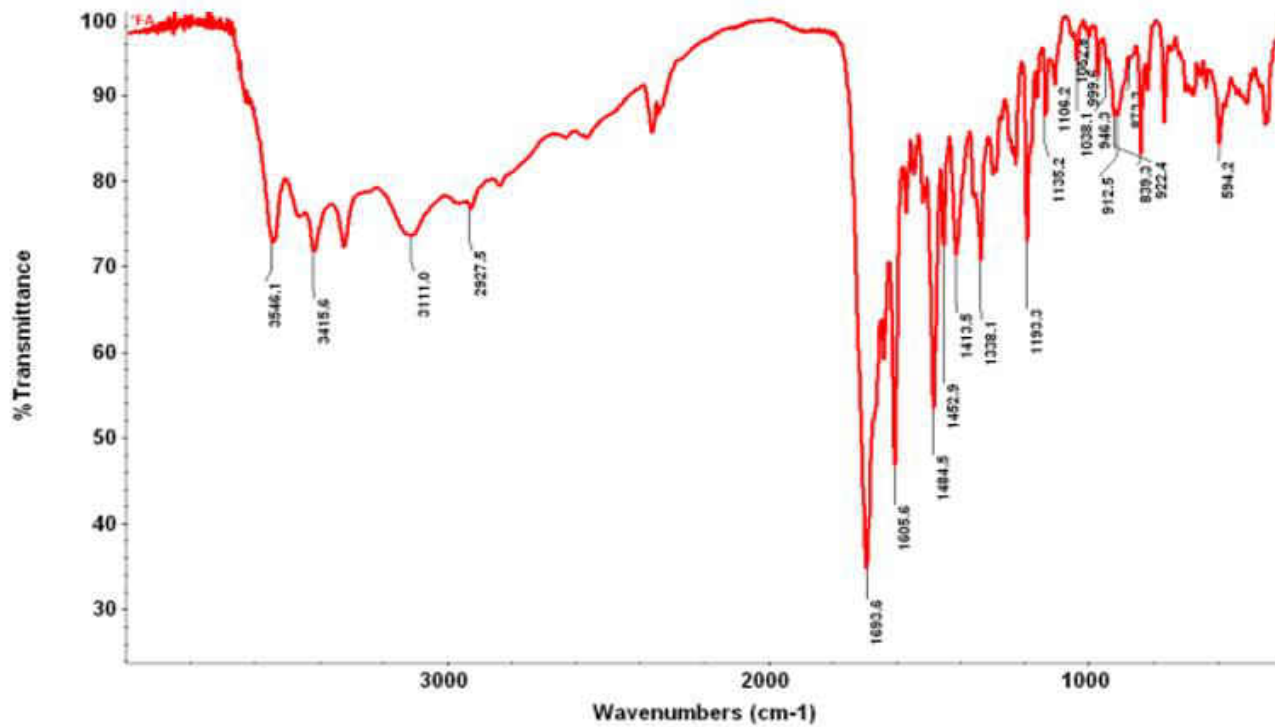


Figure 16. ATR-FTIR spectra of FA

The IR of pure FA has distinctive peaks at 3546 cm^{-1} (strong, O-H), 3415 cm^{-1} (weak, of C-H), and 1653 cm^{-1} (strong, C=O vibration).⁸⁴

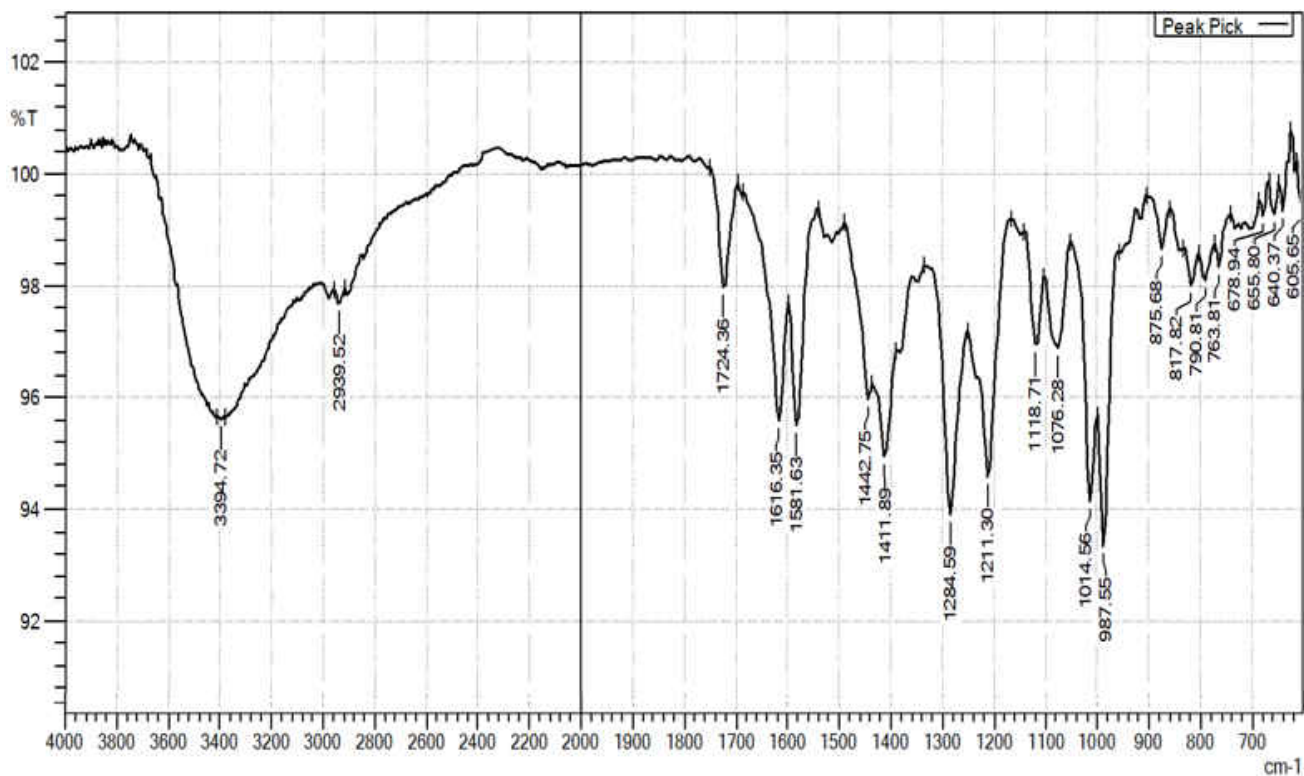


Figure 17. ATR-FTIR spectra of pure DOX

The broad peak at 33940 cm⁻¹ (strong and broad, O-H/N-H stretch), peak at 2939cm⁻¹ (weak, C-H), 1724cm⁻¹ (strong, C=O bond) 1616 cm⁻¹ and 1581 cm⁻¹ (strong, C=O and N-H), 1581 cm⁻¹ (strong, N-H), 1284 cm⁻¹ (strong, C-O-C), 1118 cm⁻¹ (strong, C-O in secondary alcohol) and 1014 cm⁻¹ (strong, C-O in primary alcohol).⁸⁵

In the covalent CDs-DOX FTIR spectrum in figure 18, there are predominant peaks at 3317 cm⁻¹, 2970 cm⁻¹, 1705 cm⁻¹, 1643 cm⁻¹, 1610 cm⁻¹, and 1076 cm⁻¹. The broad and strong peak around 3317cm⁻¹ represents the amide -NH₂ vibration peak in the covalent CDs-DOX. The strong peak at 1643 cm⁻¹ shows the presence of primary amide N-H bending while the peak at 1705cm⁻¹ represents amide C=O stretch.³⁷ These two peaks are absent in the pure CDs but are weak in the pure DOX and FA spectra.

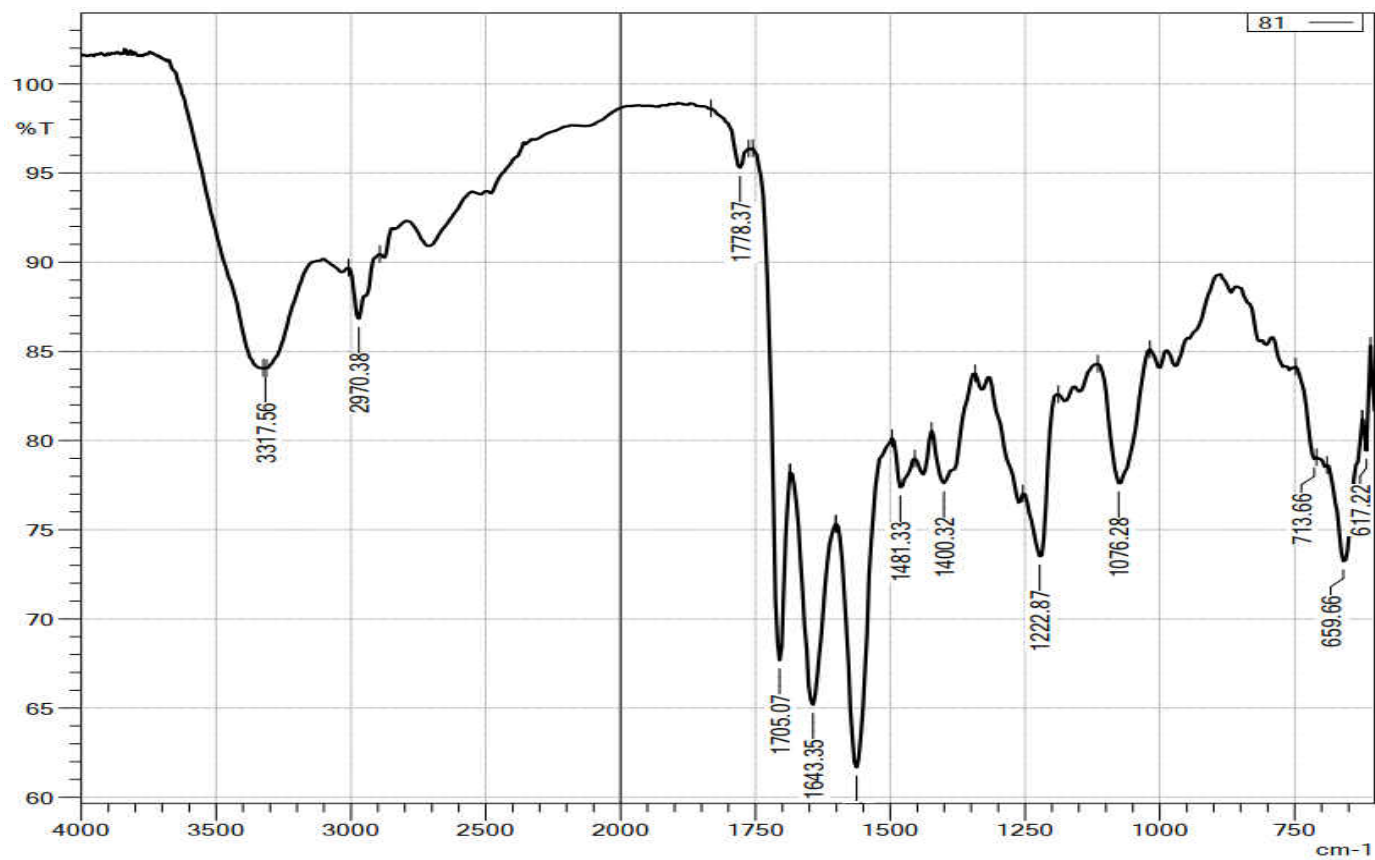


Figure 18. ATR-FTIR spectrum of covalent CDs-DOX comp

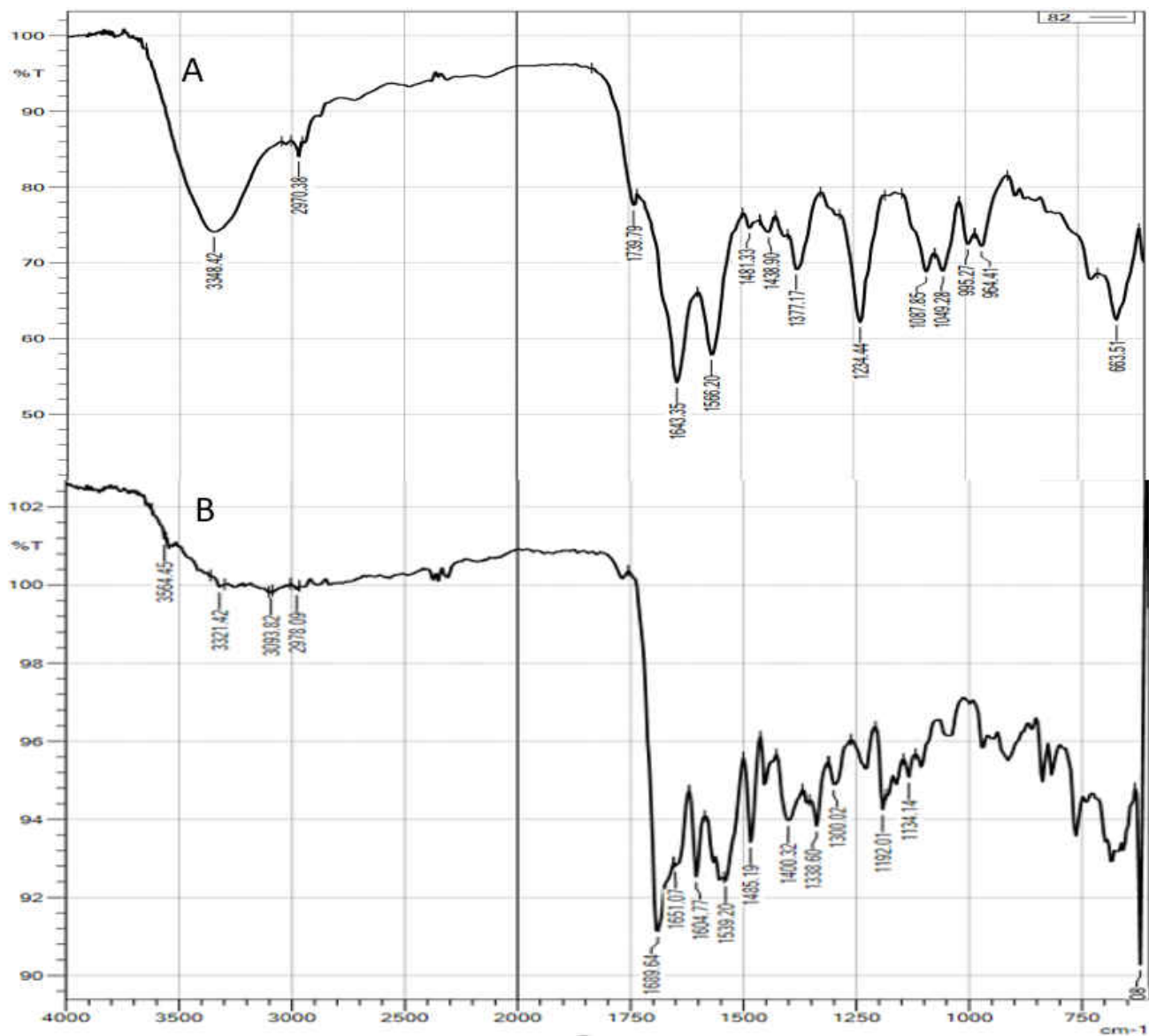


Figure 19. ATR-FTIR spectrum of covalent FA-CDs-DOX (A) and noncovalent FA-CDs-DOX complex (B)

In the covalent FA-CDs-DOX FTIR spectrum in figure 27A, the predominant peaks are at around 3348 cm⁻¹, 1643 cm⁻¹, and medium peak at 1200 and 1080 cm⁻¹. Compared to CDs, the peak around 3348 cm⁻¹ is much stronger, which may represent the vibration -NH₂ in amides. The broad and strong peaks occurring at 1643 cm⁻¹ that overlaps 1700 cm⁻¹ correspond to C=O bond

stretching in amide bond⁴² and amide primary -NH₂ bend. The peak at 1643 cm⁻¹ in the covalent complex is stronger than the NH₂ bending peak found in pure CDs, FA and DOX. This could be as a result of various amide bonds formed on different sites of the CDs surface confirming the covalent attachment of the FA, and DOX to the CDs.³³ The characteristic peaks at 1234.44cm⁻¹ and 1481 cm⁻¹ show the presence of C-N stretching vibration in typical amide bonds.⁸⁶ This peak is also stronger in the covalent complex and very weak in the pure samples (CDs, FA, and DOX). Such peak is also much stronger in FA-CD-DOX than in CDs-DOX covalent complex, it can be implied that the bond formed occur with FA and DOX both, than just with DOX alone. The peaks of C=O, C-N, and C(O)N-H in the FA-CDs-DOX spectrum further indicate the covalent bonding between FA-CDs and CDs-DOX.⁸²

The FTIR spectra for the noncovalent FA-CDs-DOX show very different peak characteristics compared to covalent FA-CDs-DOX. In the noncovalent FA-CDs-DOX in figure 19B, the peaks around 3300 cm⁻¹ representing the O-H bond in the carboxylic acid group There may be few amide groups, the -NH₂ in amide peak may be covered by the -OH group peak. The peak around 1200cm⁻¹ in the noncovalent complex spectra is much weaker, which indicates the C-N bond is much less in the noncovalent complex. All the above data in the IR spectrum of the covalent complex confirm the successful synthesis of the covalent series.

FTIR for GEM Nanoparticle

FTIR spectra for CDs-GEM and FA-CDs-GEM show similar peaks as seen in figure 21A and 27B respectively. The broad and strong peaks at 3352.28 cm⁻¹ and 3275.13 cm⁻¹ show the presence of -OH and -NH₂ in amide stretch. The peaks are broader than in several -OH peaks in the pure GEM. The new peaks at 1697 in cm⁻¹ in both complexes show carbonyl group in the amide bond.^{43,87} The strong peak at 1728 cm⁻¹ in GEM does not show up in the IR spectra of

another two complexes. Instead, the multiple strong peaks around 1635 cm^{-1} and 1647 cm^{-1} may be due to the overlay of the -C=O bond and -N-H bending in amides.³⁶ The broad peak around 1200 cm^{-1} may be the characteristic peaks of C-N stretch vibration in amide bond, which is comparable stronger in FA-CDs-GEM complex.^{15,40} This C-N peak is very weak in CDs, FA, and pure GEM. This peak might be a new bond form during the covalent synthesis of two covalent complexes.

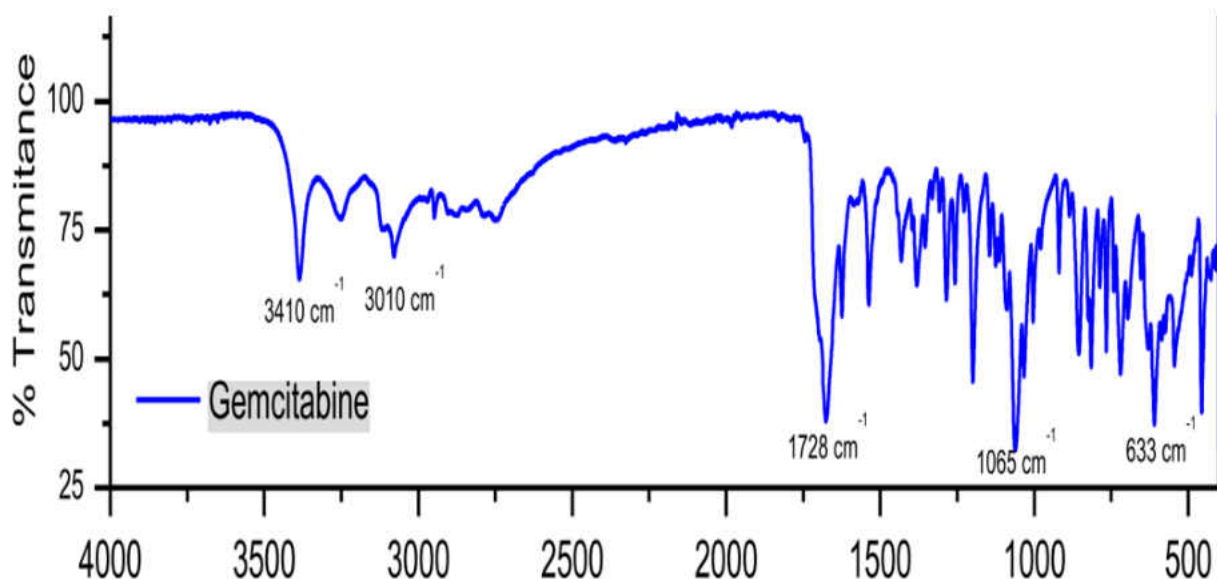


Figure 20. ATR-FTIR spectra of pure GEM

The narrow and weak peak at 3410 cm^{-1} (strong and narrow for O-H vibration) and 3010 cm^{-1} (weak, O-H) The peak at 1728 cm^{-1} (strong and broad, C=O).

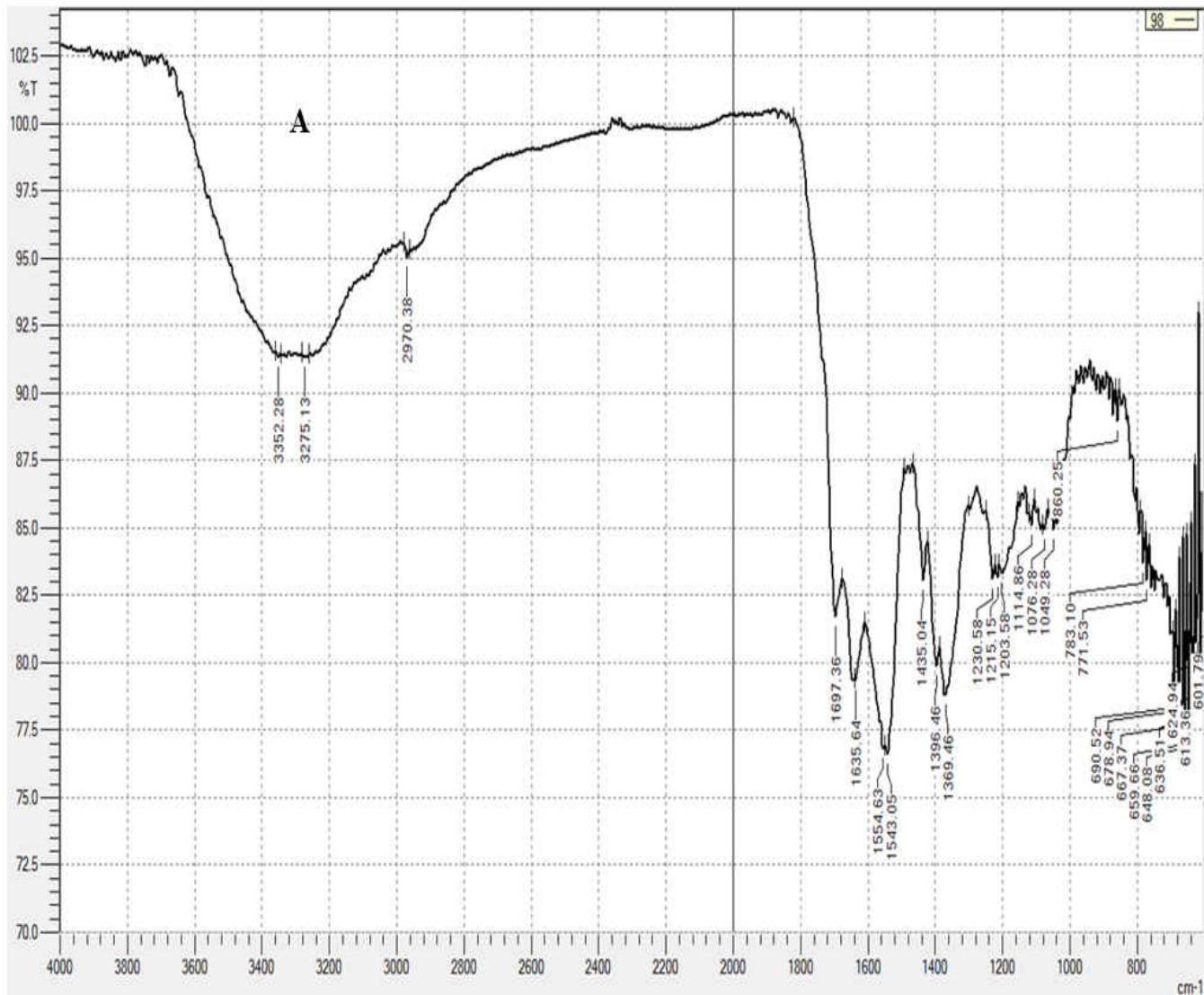


Figure 21 (continued on the next page)

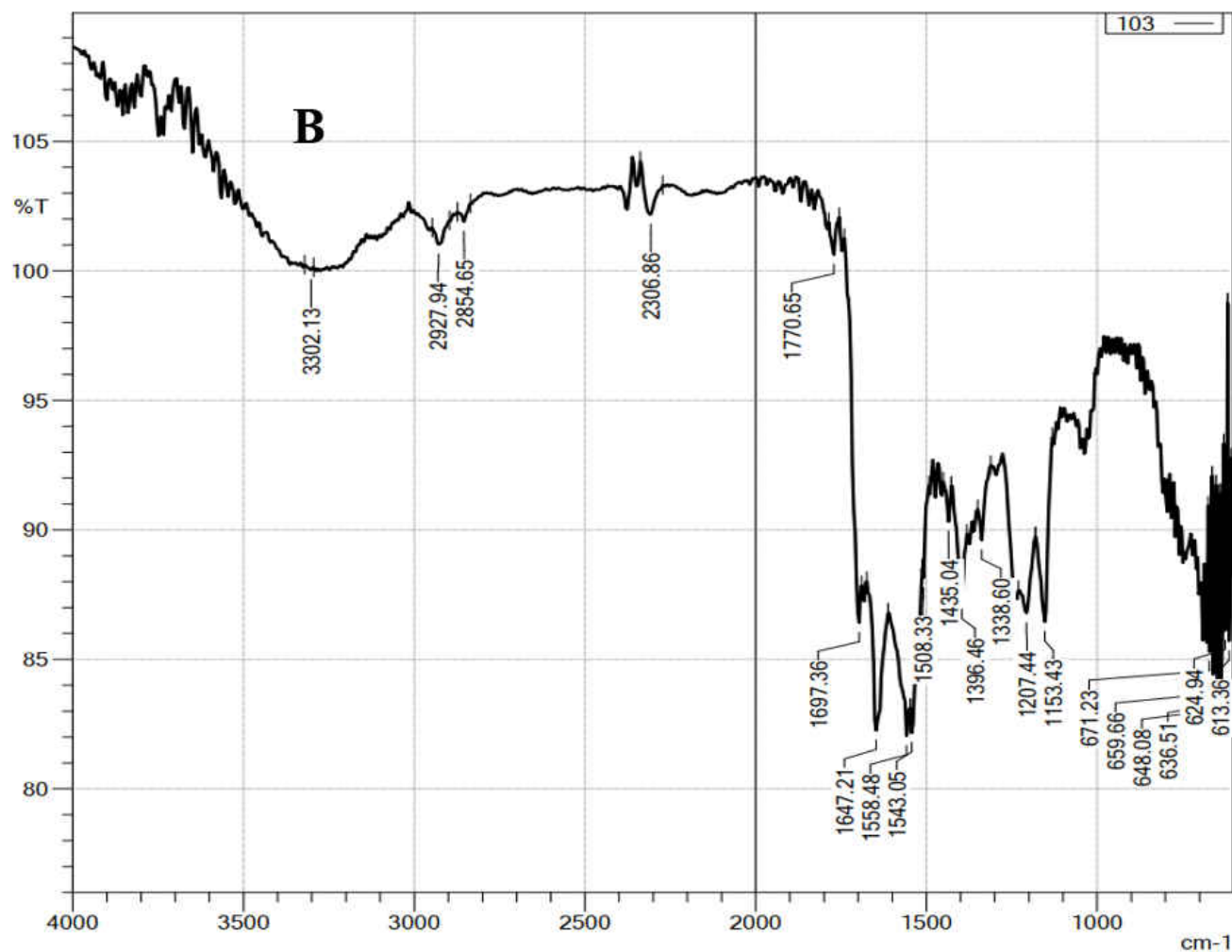


Figure 21. ATR-FTIR spectra of CDs-GEM (A) and FA-CDs-GEM (B)

Drug Loading Profile

One of the most appreciable properties of CDs is the presence of different chemical groups on the CDs surface. This makes the CDs undergo different reactions with other chemical compounds like DOX. The noncovalent attachment of drugs to CDs is usually reported with a high drug loading efficiency than when drugs are attached via covalent. However, there is limited reports on the DLE % and DLC % from the covalent attachment of DOX to CDs. The DLE % and the DLC % for our prepared noncovalent FA-CDs-DOX were calculated to be

83.8% and 3.9% respectively while the new covalent FA-CDs-DOX 71% and 80% respectively. The DLE % and the DLC % for the noncovalent CDs-DOX were also found to be 75% and 7.03% respectively. However, in the covalent CDs-DOX, the DLE% and the DLC% were calculated to be 53.7 % and 60 % with the DLE% consistent with a similar by Yang Et al.⁸⁴ that reported 52.8% for DLE%. Even though the loading efficiency in the covalent series is relatively low, the loading content is much higher. According to Shen Et al.,⁸⁸ the changes in the chemical, physical, and chemical properties during processes like covalent bonding result in nanocarriers with high drug loading content which is difficult to achieve during electrostatic drug interactions. The higher DLC might be due to the increase in the space capacity of the CDs enhanced by the covalent synthesis.⁸⁸ The DLE and the DLC for covalent FA-CDs-GEM were reported to be 69.6% and 37.8% respectively while for CDs-GEM was also calculated to be 75.1% and 46.9%. The calculation of the DLE % and DLC % was based on equation 1. Even though the DLE in the noncovalent series is higher than in the covalent series, the DLC % on the CDs is lower. The relatively higher DLC % in the covalent series might be a result of the attachment of the drug via covalent bonding. The drug loading analysis shows that the DOX covalent complexes have high DLE% and DLC% than in the GEM complex.

pH-sensitive Drug Release For Noncovalent FA-CDs-DOX

To explore the drug release profile of the complex, 2.0 mL of the complex was dialyzed in MWCO = 1.0 KDa dialysis tube against 100 mL phosphate-buffered saline (PBS) at pH 7.4 for 72 hours. The same setup was done for a pH of 5.0. In some hour's intervals (1 hr, 2hrs, 4 hrs, 7 hrs, 12 hrs, 22 hrs, 22 hrs 46 hrs, and 72 hrs), 1.0 mL of the release medium was taken and replaced with an equal volume of the buffer. The UV – vis analysis was done on the collected released medium where the absorbance at 485 nm represented the released DOX. The

concentration of the sample was calculated using the DOX calibration curve to determine the concentration DOX. The amount of drug in the released medium was determined using excel with the formula below. The same procedure was followed with the GEM complex. However, in this step, absorbance at 269nm of the free GEM was recorded for the calculation.

Amount of drug = Concentration (mg/mL) × Volume of medium (mL) × dilution factor.

% cumulative drug release (CDR) = amount of drug (mg) / theoretical drug amount (mg) × 100.^{76,81}

In an effect to mimic the cancer cell environment and the environment of a healthy cell, two PBS solutions of different pH were prepared to monitor the drug release behavior of the nanoparticles. For the pH-dependent DOX release test shown in figure 22, the noncovalent FA-CDs-DOX solutions released the highest amount of the bonded DOX at pH 5.0 (72.5% at 72 hrs) than at 7.4 (22.7% after 72 hrs). This signifies that the noncovalent FA-CDs-DOX complexes can specifically release the DOX into low pH environments.

It is reported that most solid tumors such as human breast cancer cells have low pH of 5.0 while the physiological environments have a pH of 7.4. This property of the noncovalent FA-CDs-DOX is a desirable advantage in enhancing the efficiency of cancer chemotherapy. From figure 22, the DOX was released started around 10 hours and up to 72 hours. These two properties indicate that the noncovalent FA-CDs-DOX has the capacity for selective DOX release and the possibility to provide prolonged DOX release resulting in an extended period for therapeutic effect.

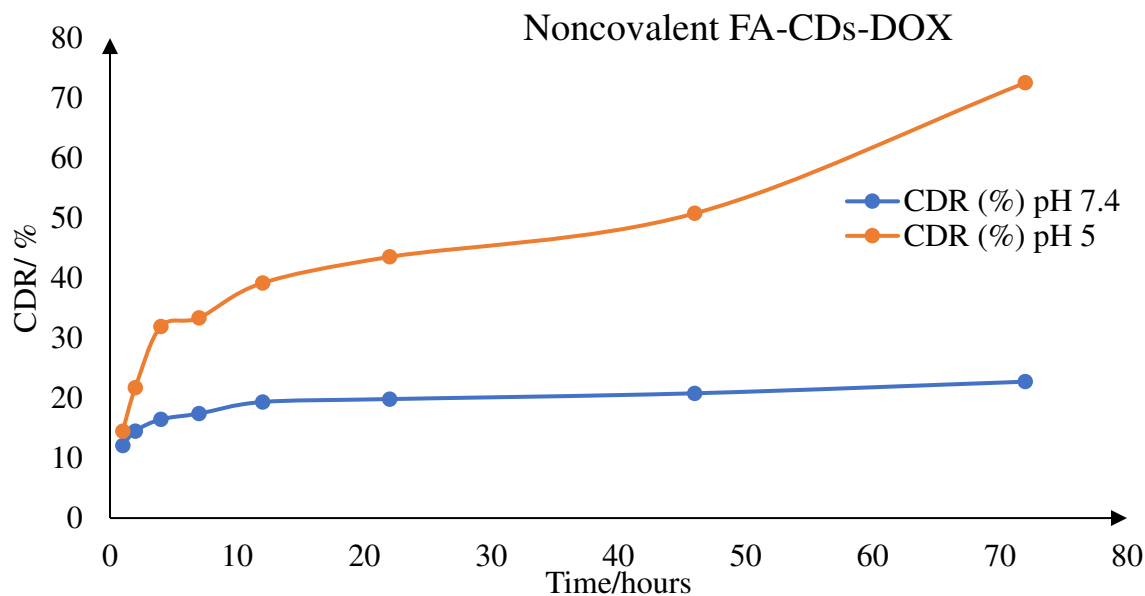


Figure 22. Graph showing the drug released in vitro at regular intervals at pH 5.0 and 7.4 phosphate-buffered saline (PBS)

However, in the covalent FA-CDs-DOX complex relatively low amount of the DOX was released as seen in figure 23. The highest quantity of DOX release after 72 hours was 44.9% at a pH of 5.0 and 16.3% at a pH of 7.4. The drug release from this complex is also moderate unlike observed in the nonvalent FA-CDs-DOX. The moderate release might be due to the strong and stable covalent bond formed between the DOX and the CDs. This low drug releases the DOX is due to the strong and stable covalent bond in the complex. The effective drug release may through other ways, such as enzyme, ligan exchange, photo-induced drug release, bond reduction, and thermal bond breakage.²⁵

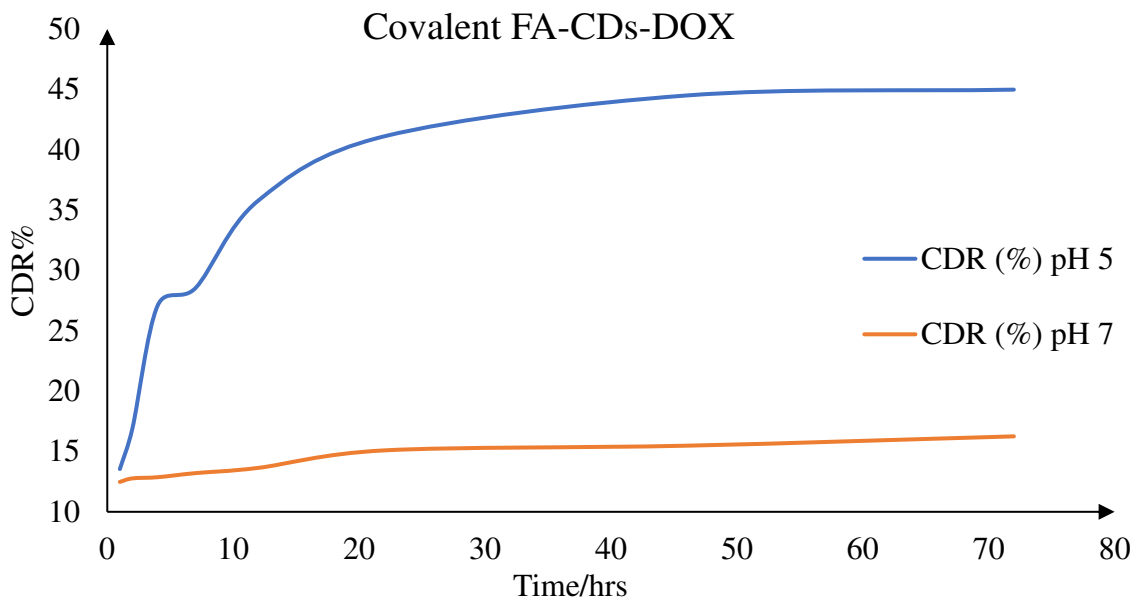


Figure 23. Graph showing the in vitro DOX released at regular intervals at pH 5.0 and 7.4 phosphate-buffered saline (PBS)

A similar trend as noncovalent FA-CDs-DOX was seen in the covalent FA-CDs-GEM in figure 24, where the higher quantity of the GEM was release in the acidic condition than in the slightly alkaline condition. The highest GEM release after 72 hours was 44.2% at pH of 5.0 and 26.5% at pH of 7.4 as depicted in figure 24. The results showed a good specificity of the FA-CDs-GEM complex for cancer cells with lower pH.

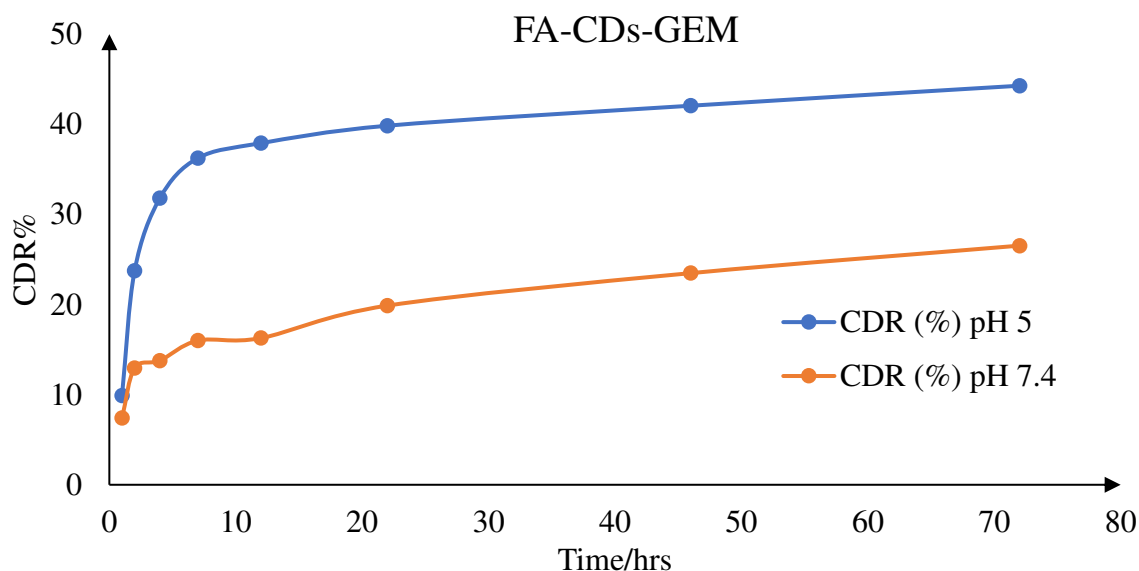


Figure 24. Graph showing the in vitro GEM released at regular intervals at pH 5.0 and 7.4 phosphate-buffered saline (PBS)

Cell Viability Assay

To investigate the efficacy of the as-prepared complexes on the tumor cells, in vitro viability test was conducted. In this study, a severe human breast cancer cell line MDA-MB-468 was used. The viability studies were conducted using Alamar Blue assay. In this analysis, the fluorescence is directly proportional to cell quantity. Therefore, the cell viability was calculated from the equation: $(A_{\text{treatment}} - A_{\text{blank}})/(A_{\text{control}} - A_{\text{blank}}) \times 100\%$. In the equation, A is the absorbance at 590 nm, $A_{\text{treatment}}$ is the absorbance of the cell line with drugs/complex, A_{blank} is the absorbance of the media, A_{control} is the absorbance of the cell line without any treatment.^{89,90} The cell viability of pure DOX, covalent, and noncovalent FA-CDs-DOX against the MDA-MB468 cell lines is shown in Figures 25 and 26. In figure 25, the cell viability with the free DOX with respect to the DOX complexes was lower at all the exposure concentrations. According to the data, the noncovalent FA-bound complex had higher efficacy toward the MDA-

MB468 cells than the covalent complexes. This observation might be due to the low release rate of the DOX from the strong stable amide bond in the covalent complex. In all the FA bounded complexes and the covalent CDs-DOX, considerably high cell death was observed than in the noncovalent CDs-DOX. The FA bounded complexes will be much preferred since the FA can help target the cancer cells than healthy cells. The viability test on the MDA-MB-468 suggests that all the FA bounded complexes can potentially be used as a drug candidate for invasive breast cancers such as MDA-MB-468.

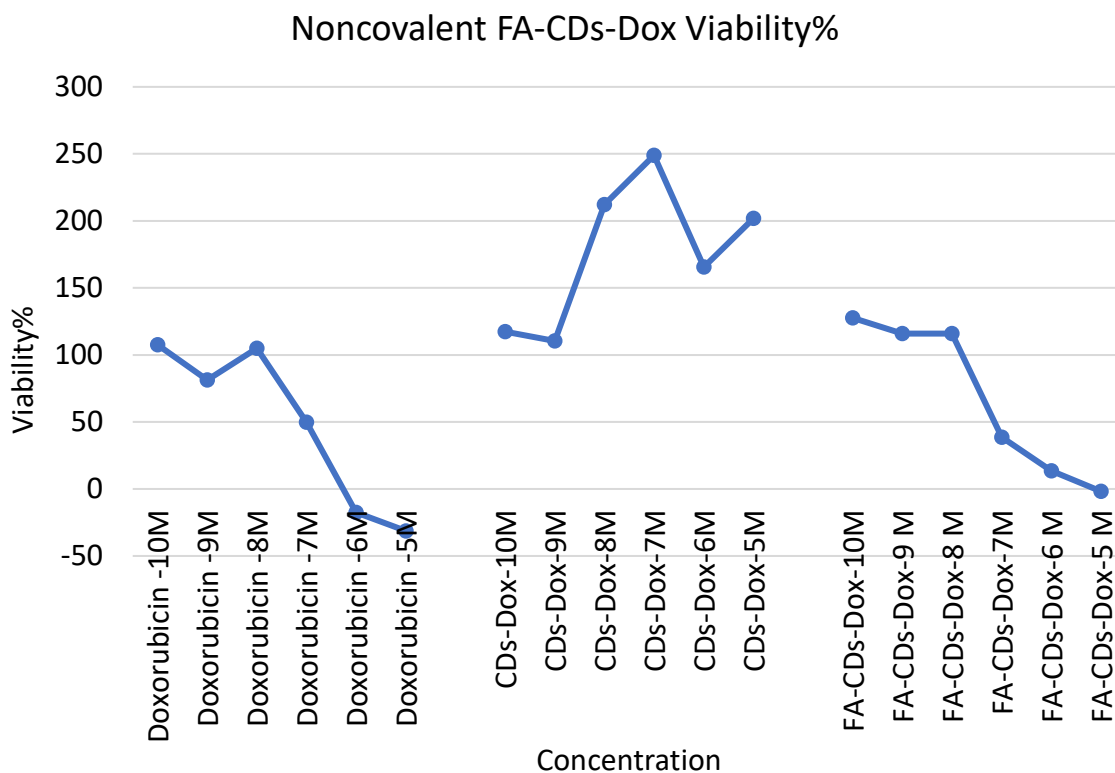


Figure 25. Cell viability of MDA-MB-468 cells exposed to free DOX, noncovalent CDs-DOX, and noncovalent FA-CDs-DOX at 72 h

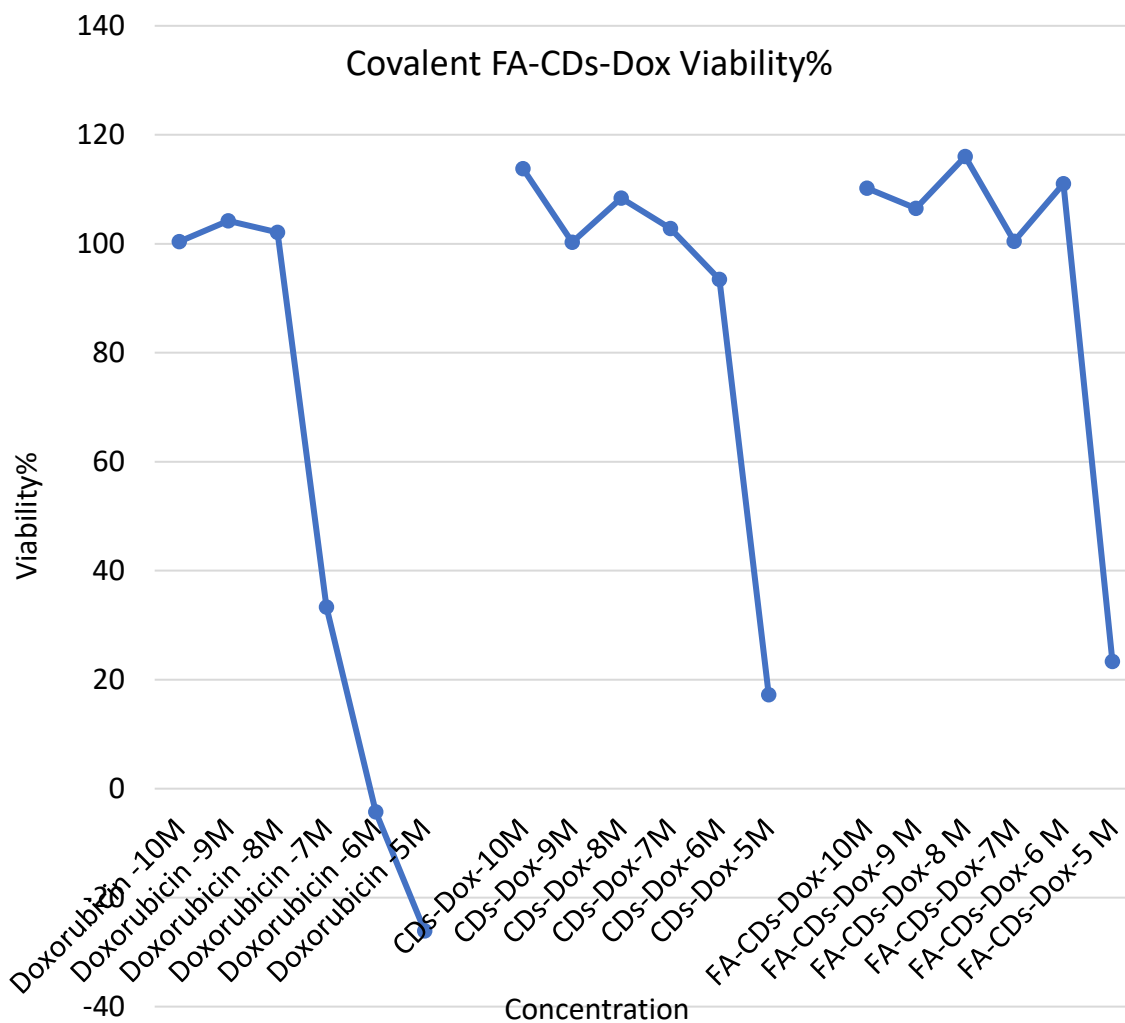


Figure 26. Cell viability of MDA-MB-468 cells exposed to free DOX, covalent CDs-DOX, and covalent FA-CDs-DOX at 72 h

CHAPTER 4. CONCLUSION

I successfully prepared covalent and noncovalent FA-CDs-DOX and covalent FA-CDs-GEM. Also, the UV-vis, fluorescence, and IR spectra for the CDs, FA, covalent and noncovalent FA-CDs-DOX, and the covalent FA-CDs-GEM were compared to confirm the successful fabrication of NPs complexes. According to the data from VT, the sizes of all NPs synthesized is between 2 nm and 5 nm. The in vitro drug release data show that the noncovalent FA-CDs-DOX can efficiently release the drug in acidic conditions than in the covalent series. The covalent FA-CDs-GEM had relatively moderate drug release in the acidic environment. The drug loading profile shows high DLC in both covalent FA-CDs-GEM and FA-CDs-DOX complexes than the noncovalent series of FA-CDs-DOX. However, there is higher DLE in the noncovalent series than in all the covalent complexes. The cell viability against MDA-MB468 cancer cells proved both covalent and non-covalent FA-CDs-DOX are more specific than the NPs without FA. More cell viability test is being done by our collaborators from the pharmaceutical department at ETSU and Xavier University at Louisiana. For further studies, the cytotoxicity of the complexes on different types of cancer cell lines will be explored. We will investigate other methods of attaching the DOX/GEM to the CDs. We will then consider preparing FA-CDs-based combinational chemotherapy (DOX and GEM) – the possibility to increase the overall therapeutic effect.

REFERENCES

- (1) Mohammadi, S.; Salimi, A.; Hamd-Ghadareh, S.; Fathi, F.; Soleimani, F. A FRET Immunosensor for Sensitive Detection of CA 15-3 Tumor Marker in Human Serum Sample and Breast Cancer Cells Using Antibody Functionalized Luminescent Carbon-Dots and AuNPs-Dendrimer Aptamer as Donor-Acceptor Pair. *Anal. Biochem.* **2018**, *557* (June), 18–26. <https://doi.org/10.1016/j.ab.2018.06.008>.
- (2) Estimated Number of New Cases in 2018 , Worldwide , All Cancers , Both Sexes , All Ages. *Glob. Cancer Obs.* **2018**, *849*, 2018.
<https://doi.org/https://gco.iarc.fr/today/data/factsheets/populations/900-world-factsheets.pdf>.
- (3) Baskar, R.; Lee, K. A.; Yeo, R.; Yeoh, K. W. Cancer and Radiation Therapy: Current Advances and Future Directions. *Int. J. Med. Sci.* **2012**, *9* (3), 193–199.
<https://doi.org/10.7150/ijms.3635>.
- (4) Tohme, S.; Simmons, R. L.; Tsung, A. Surgery for Cancer: A Trigger for Metastases. *Cancer Res* **2018**, *77* (7), 1548–1552. <https://doi.org/10.1158/0008-5472.CAN-16-1536.Surgery>.
- (5) Hu, Q.; Sun, W.; Wang, C.; Gu, Z. Recent Advances of Cocktail Chemotherapy by Combination Drug Delivery Systems. *Adv. Drug Deliv. Rev.* **2016**, *98*, 19–34.
<https://doi.org/10.1016/j.addr.2015.10.022>.
- (6) Wulfschle, J. D.; Liotta, L. A.; Petricoin, E. F. Proteomic Applications for the Early Detection of Cancer. *Nat. Rev. Cancer* **2003**, *3* (4), 267–275.
<https://doi.org/10.1038/nrc1043>.

- (7) Williams, P. A. A Productive History and Physical Examination in the Prevention and Early Detection of Cancer. *Cancer* **1981**, *47* (5 Suppl), 1146–1150.
- (8) Tomasi, T. B. Structure and Function of Alpha-Fetoprotein. *Annu. Rev. Med.* **1977**, *28* (1), 453–465. <https://doi.org/10.1146/annurev.me.28.020177.002321>.
- (9) Tipa, R.; Tipa, R.; Baltag, O.; Baltag, O. Microwave Thermography for Cancer Detection. *Rom. J. Phys.* **2006**, *51* (3–4), 371–377.
- (10) Piccardo, A.; Paparo, F.; Piccazzo, R.; Naseri, M.; Ricci, P.; Marziano, A.; Bacigalupo, L.; Biscaldi, E.; Rollandi, G. A.; Grillo-Ruggieri, F.; Farsad, M. Erratum: Value of Fused 18F-Choline-PET/MRI to Evaluate Prostate Cancer Relapse in Patients Showing Biochemical Recurrence after EBRT: Preliminary Results (BioMed Research International (2014) 2014). *Biomed Res. Int.* **2016**, *2016*, 2–9. <https://doi.org/10.1155/2016/5047948>.
- (11) Jing, H.; Li, F.; Zhuang, H.; Wang, Z.; Tian, J. Effective Detection of the Tumors Causing Osteomalacia Using [Tc-99m] -HYNIC-Octreotide (^{99m}Tc-HYNIC-TOC) Whole Body Scan. *Eur. J. Radiol.* **2013**, *82* (11), 2028–2034. <https://doi.org/10.1016/j.ejrad.2013.04.006>.
- (12) Grab, D.; Flock, F.; Sto, I.; Nu, K.; Rieber, A.; Fenchel, S.; Reske, S. N.; Kreienberg, R. Classification of Asymptomatic Adnexal Masses by Ultrasound , Magnetic Resonance Imaging , and Positron Emission Tomography. *Gynecol. Oncol.* **2000**, *459* (77), 454–459. <https://doi.org/10.1006/gyno.2000.5768>.
- (13) Choi, H. J.; Ju, W.; Myung, S. K.; Kim, Y. Magnetic Resonance Imaging , and Positron Emission Computer Tomography for Detection of Metastatic Lymph Nodes in Patients with Cervical Cancer : *Cancer Sci.* **2010**, *101* (6), 1471–1479.

<https://doi.org/10.1111/j.1349-7006.2010.01532.x>.

- (14) Tao, H.; Yang, K.; Ma, Z.; Wan, J.; Zhang, Y.; Kang, Z. In Vivo NIR Fluorescence Imaging , Biodistribution , and Toxicology of Photoluminescent Carbon Dots Produced from Carbon Nanotubes and Graphite. *Small* **2012**, 8 (2), 281–290.
<https://doi.org/10.1002/sml.201101706>.
- (15) Yuan, Y.; Guo, B.; Hao, L.; Liu, N.; Lin, Y.; Guo, W.; Li, X.; Gu, B. Doxorubicin-Loaded Environmentally Friendly Carbon Dots as a Novel Drug Delivery System for Nucleus Targeted Cancer Therapy. *Colloids Surfaces B Biointerfaces* **2017**, 159, 349–359.
<https://doi.org/10.1016/j.colsurfb.2017.07.030>.
- (16) Nurgali, K.; Jagoe, R. T.; Abalo, R. Editorial : Adverse Effects of Cancer Chemotherapy : Anything New to Improve Tolerance and Reduce Sequelae ? **2018**, 9 (March), 1–3.
<https://doi.org/10.3389/fphar.2018.00245>.
- (17) Peer, D.; Karp, J. M.; Hong, S.; Farokhzad, O. C.; Margalit, R.; Langer, R. Nanocarriers as an Emerging Platform for Cancer Therapy. *Nat. Nanotechnol.* **2007**, 2 (12), 751–760.
<https://doi.org/10.1038/nnano.2007.387>.
- (18) Kibria, G.; Hatakeyama, H. Cancer Multidrug Resistance : Mechanisms Involved and Strategies for Circumvention Using a Drug Delivery System. *Arch. Pharm. Res.* **2014**, 37 (1), 4–15. <https://doi.org/10.1007/s12272-013-0276-2>.
- (19) Al-Lazikani, B.; Banerji, U.; Workman, P. Combinatorial Drug Therapy for Cancer in the Post-Genomic Era. *Nat. Biotechnol.* **2012**, 30 (7), 679–692.
<https://doi.org/10.1038/nbt.2284>.

- (20) Hu, C. M. J.; Zhang, L. Nanoparticle-Based Combination Therapy toward Overcoming Drug Resistance in Cancer. *Biochem. Pharmacol.* **2012**, *83* (8), 1104–1111.
<https://doi.org/10.1016/j.bcp.2012.01.008>.
- (21) Mansoori, B.; Mohammadi, A.; Davudian, S.; Shirjang, S.; Baradaran, B. The Different Mechanisms of Cancer Drug Resistance: A Brief Review. *Adv. Pharm. Bull.* **2017**, *7* (3), 339–348. <https://doi.org/10.15171/apb.2017.041>.
- (22) Pandey, S.; Gedda, G. R.; Thakur, M.; Bhaisare, M. L.; Talib, A.; Khan, M. S.; Wu, S. M.; Wu, H. F. Theranostic Carbon Dots ‘Clathrate-like’ Nanostructures for Targeted Photo-Chemotherapy and Bioimaging of Cancer. *J. Ind. Eng. Chem.* **2017**, *56*, 62–73.
<https://doi.org/10.1016/j.jiec.2017.06.008>.
- (23) Priya James, H.; John, R.; Alex, A.; Anoop, K. R. Smart Polymers for the Controlled Delivery of Drugs – a Concise Overview. *Acta Pharm. Sin. B* **2014**, *4* (2), 120–127.
<https://doi.org/10.1016/j.apsb.2014.02.005>.
- (24) Gurunathan, S.; Kang, M. H.; Qasim, M.; Kim, J. H. Nanoparticle-Mediated Combination Therapy: Two-in-One Approach for Cancer. *Int. J. Mol. Sci.* **2018**, *19* (10), 1–37.
<https://doi.org/10.3390/ijms19103264>.
- (25) Doane, T.; Burda, C. Nanoparticle Mediated Non-Covalent Drug Delivery. *Adv. Drug Deliv. Rev.* **2013**, *65* (5), 607–621. <https://doi.org/10.1016/j.addr.2012.05.012>.
- (26) Morachis, J. M.; Mahmoud, E. A.; Almutairi, A. Physical and Chemical Strategies for Therapeutic Delivery by Using Polymeric Nanoparticles. *Pharmacol. Rev.* **2012**, *64* (3), 505–519. <https://doi.org/10.1124/pr.111.005363>.

- (27) Öztekin Long, Nicole, M and Badre, D. Deep Penetration of a PDT Drug into Tumors by Non-Covalent Drug-Gold Nanoparticle Conjugates. *Bone* **2008**, *23* (1), 1–7.
<https://doi.org/10.1038/jid.2014.371>.
- (28) Farshbaf, M.; Davaran, S.; Rahimi, F.; Annabi, N.; Salehi, R.; Akbarzadeh, A. Carbon Quantum Dots: Recent Progresses on Synthesis, Surface Modification and Applications. *Artif. Cells, Nanomedicine Biotechnol.* **2018**, *46* (7), 1331–1348.
<https://doi.org/10.1080/21691401.2017.1377725>.
- (29) Yong, K.-T. Quantum Dots for Biophotonics. *Theranostics* **2012**, *2* (7), 629–630.
<https://doi.org/10.7150/thno.4757>.
- (30) Mo, D.; Hu, L.; Zeng, G.; Chen, G.; Wan, J.; Yu, Z.; Huang, Z.; He, K.; Zhang, C.; Cheng, M. Cadmium-Containing Quantum Dots: Properties, Applications, and Toxicity. *Appl. Microbiol. Biotechnol.* **2017**, *101* (7), 2713–2733. <https://doi.org/10.1007/s00253-017-8140-9>.
- (31) Matea, C. T.; Mocan, T.; Tabaran, F.; Pop, T.; Mosteanu, O.; Puia, C.; Iancu, C.; Mocan, L. Quantum Dots in Imaging, Drug Delivery and Sensor Applications. *Int. J. Nanomedicine* **2017**, *12*, 5421–5431. <https://doi.org/10.2147/IJN.S138624>.
- (32) Luo, Pengju G., Sushant Sahu, Sheng-Tao Yang, Sumit K. Sonkar, Jinping Wang, Haifang Wang, Gregory E. LeCroy, Li Cao, and Y.-P. S. Carbon “Quantum” Dots for Optical Bioimaging. *J. Mater. Chem. B* **2013**, *6* (November 2016), 2116–2127.
<https://doi.org/10.1039/C3TB00018D>.
- (33) Zhu, S.; Meng, Q.; Wang, L.; Zhang, J.; Song, Y.; Jin, H.; Zhang, K.; Sun, H.; Wang, H.; Yang, B. Highly Photoluminescent Carbon Dots for Multicolor Patterning, Sensors, and

- Bioimaging. *Angew. Chemie - Int. Ed.* **2013**, *52* (14), 3953–3957.
<https://doi.org/10.1002/anie.201300519>.
- (34) Hola, K.; Zhang, Y.; Wang, Y.; Giannelis, E. P.; Zboril, R.; Rogach, A. L. Carbon Dots —
— Emerging Light Emitters for Bioimaging , Cancer Therapy and Optoelectronics. *Nano
Today* **2014**, *9* (5), 590–603. <https://doi.org/10.1016/j.nantod.2014.09.004>.
- (35) Wu, Y.; Wu, H.; Kuan, C.; Lin, C.; Wang, L.; Chang, C.; Wang, T. Multi-Functionalized
Carbon Dots as Theranostic Nanoagent for Gene Delivery in Lung Cancer Therapy. *Nat.
Publ. Gr.* **2016**, *6* (January), 1–12. <https://doi.org/10.1038/srep21170>.
- (36) Hao, L.; Wei, Y.; Cai, X.; Zhu, B. Doxorubicin Conjugated Carbon Dots as a Drug
Delivery System for Human Breast Cancer Therapy. *Cell Prolif.* **2018**, *51*, e12488.
<https://doi.org/10.1111/cpr.12488>.
- (37) Mewada, A.; Pandey, S.; Thakur, M.; Jadhav, D.; Sharon, M. Swarming Carbon Dots for
Folic Acid Mediated Delivery of Doxorubicin and Biological Imaging. *J. Mater. Chem. B*
2014, *2* (6), 698–705. <https://doi.org/10.1039/c3tb21436b>.
- (38) Boakye-Yiadom, K. O.; Kesse, S.; Opoku-Damoah, Y.; Filli, M. S.; Aquib, M.; Joelle, M.
M. B.; Farooq, M. A.; Mavlyanova, R.; Raza, F.; Bavi, R.; Wang, B. Carbon Dots:
Applications in Bioimaging and Theranostics. *Int. J. Pharm.* **2019**, *564* (April), 308–317.
<https://doi.org/10.1016/j.ijpharm.2019.04.055>.
- (39) Meiling, T. T. Development of a Reliable and Environmentally Friendly Synthesis for
Fluorescence Carbon Nanodots. *Univ. Potsdam* **2017**, 25–198.
- (40) Li, S.; Wang, L.; Chusuei, C. C.; Suarez, V. M.; Blackwelder, P. L.; Micic, M.;

- Orbulescu, J.; Leblanc, R. M. Nontoxic Carbon Dots Potently Inhibit Human Insulin Fibrillation. *Chem. Mater.* **2015**, *27* (5), 1764–1771. <https://doi.org/10.1021/cm504572b>.
- (41) Pardo, J.; Peng, Z.; Leblanc, R. M. Cancer Targeting and Drug Delivery Using Carbon-Based Quantum Dots and Nanotubes. *Molecules* **2018**, *23* (2), 1–20. <https://doi.org/10.3390/molecules23020378>.
- (42) Wu, Y. F.; Wu, H. C.; Kuan, C. H.; Lin, C. J.; Wang, L. W.; Chang, C. W.; Wang, T. W. Multi-Functionalized Carbon Dots as Theranostic Nanoagent for Gene Delivery in Lung Cancer Therapy. *Sci. Rep.* **2016**, *6* (October 2015), 1–12. <https://doi.org/10.1038/srep21170>.
- (43) Ghosh, S.; Ghosal, K.; Mohammad, S. A.; Sarkar, K. Dendrimer Functionalized Carbon Quantum Dot for Selective Detection of Breast Cancer and Gene Therapy. *Chem. Eng. J.* **2019**, *373* (April), 468–484. <https://doi.org/10.1016/j.cej.2019.05.023>.
- (44) Li, S.; Jiang, J.; Yan, Y.; Wang, P.; Huang, G.; Kim, N. hoon; Lee, J. H.; He, D. Red, Green, and Blue Fluorescent Folate-Receptor-Targeting Carbon Dots for Cervical Cancer Cellular and Tissue Imaging. *Mater. Sci. Eng. C* **2018**, *93* (August), 1054–1063. <https://doi.org/10.1016/j.msec.2018.08.058>.
- (45) Duan, Q.; Ma, Y.; Che, M.; Zhang, B.; Zhang, Y.; Li, Y.; Zhang, W.; Sang, S. Fluorescent Carbon Dots as Carriers for Intracellular Doxorubicin Delivery and Track. *J. Drug Deliv. Sci. Technol.* **2019**, *49* (August 2018), 527–533. <https://doi.org/10.1016/j.jddst.2018.12.015>.
- (46) Mignani, S.; Bryszewska, M.; Klajnert-Maculewicz, B.; Zablocka, M.; Majoral, J. P. Advances in Combination Therapies Based on Nanoparticles for Efficacious Cancer

- Treatment: An Analytical Report. *Biomacromolecules* **2015**, *16* (1), 1–27.
<https://doi.org/10.1021/bm501285t>.
- (47) Neikov, O. D.; Yefimov, N. A. *Nanopowders*, 2nd ed.; Elsevier Ltd., 2019.
<https://doi.org/10.1016/b978-0-08-100543-9.00009-9>.
- (48) Zheng, M.; Ruan, S.; Liu, S.; Sun, T.; Qu, D.; Zhao, H.; Xie, Z.; Gao, H.; Jing, X.; Sun, Z.; Science, M.; Street, Y.; Mechanics, F.; Academy, C.; Road, E. N.; Physics, P.; Chemistry, A.; Academy, C.; Street, R.; Targeting, D.; Systems, D. D.; Road, S. R.; Academy, C.; Catalysis, G.; Engineering, C. Self-Targeting Fluorescent Carbon Dots for Diagnosis of Brain Cancer. *ACS Nano* **2015**, *9* (11), 11455–11461.
<https://doi.org/https://pubs.acs.org/doi/abs/10.1021/acs.nano.5b05575>.
- (49) Zhu, H.; Wang, X.; Li, Y.; Wang, Z.; Yang, F.; Yang, X. Microwave Synthesis of Fluorescent Carbon Nanoparticles with Electrochemiluminescence Properties. *Chem. Commun.* **2009**, No. 34, 5118–5120. <https://doi.org/10.1039/b907612c>.
- (50) Zhang, J.; Zhao, X.; Xian, M.; Dong, C.; Shuang, S. Folic Acid-Conjugated Green Luminescent Carbon Dots as a Nanoprobe for Identifying Folate Receptor-Positive Cancer Cells. *Talanta* **2018**, *183* (November 2017), 39–47.
<https://doi.org/10.1016/j.talanta.2018.02.009>.
- (51) Ghosal, K.; Ghosh, A. Carbon Dots: The next Generation Platform for Biomedical Applications. *Mater. Sci. Eng. C* **2019**, *96*, 887–903.
<https://doi.org/10.1016/j.msec.2018.11.060>.
- (52) Singh, I.; Arora, R.; Dhiman, H.; Pahwa, R. Carbon Quantum Dots: Synthesis, Characterization and Biomedical Applications. *Turkish J. Pharm. Sci.* **2018**, *15* (2), 219–

230. <https://doi.org/10.4274/tjps.63497>.
- (53) Liu, H.; Li, Z.; Sun, Y.; Geng, X.; Hu, Y.; Meng, H.; Ge, J.; Qu, L. Synthesis of Luminescent Carbon Dots with Ultrahigh Quantum Yield and Inherent Folate Receptor-Positive Cancer Cell Targetability. *Sci. Rep.* **2018**, *8* (1), 1–8. <https://doi.org/10.1038/s41598-018-19373-3>.
- (54) Bazak, R.; Hourri, M.; El Achy, S.; Kamel, S.; Refaat, T. Cancer Active Targeting by Nanoparticles: A Comprehensive Review of Literature. *J. Cancer Res. Clin. Oncol.* **2015**, *141* (5), 769–784. <https://doi.org/10.1007/s00432-014-1767-3>.
- (55) Conde, J.; Doria, G.; Baptista, P. Noble Metal Nanoparticles Applications in Cancer. *J. Drug Deliv.* **2012**, *2012*, 1–12. <https://doi.org/10.1155/2012/751075>.
- (56) Fernández, M.; Javaid, F.; Chudasama, V. Advances in Targeting the Folate Receptor in the Treatment/Imaging of Cancers. *Chem. Sci.* **2018**, *9* (4), 790–810. <https://doi.org/10.1039/c7sc04004k>.
- (57) Su, H.; Liao, Y.; Wu, F.; Sun, X.; Liu, H.; Wang, K.; Zhu, X. Cetuximab-Conjugated Iodine Doped Carbon Dots as a Dual Fluorescent/CT Probe for Targeted Imaging of Lung Cancer Cells. *Colloids Surfaces B Biointerfaces* **2018**, *170* (March), 194–200. <https://doi.org/10.1016/j.colsurfb.2018.06.014>.
- (58) Antony, A. C. Folate Receptors. *Annu. Rev. Nutr.* **1996**, *16* (1), 501–521. <https://doi.org/10.1146/annurev.nutr.16.1.501>.
- (59) Chong, C. R.; Sullivan, D. J. New Uses for Old Drugs. *Nature* **2007**, *448* (August), 645–646.

- (60) Shen, W.; Chen, X.; Luan, J.; Wang, D.; Yu, L.; Ding, J. Sustained Codelivery of Cisplatin and Paclitaxel via an Injectable Prodrug Hydrogel for Ovarian Cancer Treatment. *ACS Appl. Mater. Interfaces* **2017**, *9* (46), 40031–40046. <https://doi.org/10.1021/acsami.7b11998>.
- (61) De Verdière, A. C.; Dubernet, C.; Némati, F.; Soma, E.; Appel, M.; Ferté, J.; Bernard, S.; Puisieux, F.; Couvreur, P. Reversion of Multidrug Resistance with Polyalkylcyanoacrylate Nanoparticles: Towards a Mechanism of Action. *Br. J. Cancer* **1997**, *76* (2), 198–205. <https://doi.org/10.1038/bjc.1997.362>.
- (62) Alyane, M.; Benguedouar, L.; Kebsa, W.; Boussenane, H. N.; Rouibah, H.; Lahouel, M. Cardioprotective Effects and Mechanism of Action of Polyphenols Extracted from Propolis against Doxorubicin Toxicity. *Pak. J. Pharm. Sci.* **2008**, *21* (3), 201–209.
- (63) L'Ecuyer, T.; Sanjeev, S.; Thomas, R.; Novak, R.; Das, L.; Campbell, W.; Vander Heide, R. DNA Damage Is an Early Event in Doxorubicin-Induced Cardiac Myocyte Death. *Am. J. Physiol. - Hear. Circ. Physiol.* **2006**, *291* (3), 1273–1280. <https://doi.org/10.1152/ajpheart.00738.2005>.
- (64) Ardekani, S. M.; Dehghani, A.; Hassan, M.; Kianinia, M.; Aharonovich, I.; Gomes, V. G. Two-Photon Excitation Triggers Combined Chemo-Photothermal Therapy via Doped Carbon Nanohybrid Dots for Effective Breast Cancer Treatment. *Chem. Eng. J.* **2017**, *330* (July), 651–662. <https://doi.org/10.1016/j.cej.2017.07.165>.
- (65) Veltkamp, S.; van Eijndhoven, M.; Pluim, D.; Bolijn, M.; Jansen, R.; Garcia-Ribas, I.; Wickremsinhe, E.; Beijnen, J.; Schellens, J. Gemcitabine Metabolite, 2',2'-Difluorodeoxyuridine (DFdU), Can Be Phosphorylated and Incorporated into Nucleic

- Acids. *AACR Meet. Abstr.* **2007**, 2007 (1_Annual_Meeting), 1541.
- (66) Samanta, K.; Setua, S.; Kumari, S.; Jaggi, M.; Yallapu, M. M.; Chauhan, S. C. Gemcitabine Combination Nano Therapies for Pancreatic Cancer. *Pharmaceutics* **2019**, *11* (11), 1–25. <https://doi.org/10.3390/pharmaceutics11110574>.
- (67) Toschi, L.; Finocchiaro, G.; Bartolini, S.; Gioia, V.; Cappuzzo, F. Role of Gemcitabine in Cancer Therapy. *Futur. Oncol.* **2005**, *1* (1), 7–17. <https://doi.org/10.1517/14796694.1.1.7>.
- (68) Arsawang, U.; Saengsawang, O.; Rungrotmongkol, T.; Sornmee, P.; Wittayanarakul, K.; Remsungnen, T.; Hannongbua, S. How Do Carbon Nanotubes Serve as Carriers for Gemcitabine Transport in a Drug Delivery System? *J. Mol. Graph. Model.* **2011**, *29* (5), 591–596. <https://doi.org/10.1016/j.jmgm.2010.11.002>.
- (69) Hensley, M. L. Update on Gemcitabine and Docetaxel Combination Therapy for Primary and Metastatic Sarcomas. *Curr. Opin. Oncol.* **2010**, *22* (4), 356–361. <https://doi.org/10.1097/CCO.0b013e32833aafef>.
- (70) Kose, M. F.; Meydanli, M. M.; Tulunay, G. Gemcitabine plus Carboplatin in Platinum-Sensitive Recurrent Ovarian Carcinoma. *Expert Rev. Anticancer Ther.* **2006**, *6* (3), 437–443. <https://doi.org/10.1586/14737140.6.3.437>.
- (71) Schneider, J.; Reckmeier, C. J.; Xiong, Y.; Von Seckendorff, M.; Susha, A. S.; Kasak, P.; Rogach, A. L. Molecular Fluorescence in Citric Acid-Based Carbon Dots. *J. Phys. Chem. C* **2017**, *121* (3), 2014–2022. <https://doi.org/10.1021/acs.jpcc.6b12519>.
- (72) Liyanage, P. Y.; Zhou, Y.; Al-Youbi, A. O.; Bashammakh, A. S.; El-Shahawi, M. S.; Vanni, S.; Graham, R. M.; Leblanc, R. M. Pediatric Glioblastoma Target-Specific

- Efficient Delivery of Gemcitabine across the Blood-Brain Barrier: Via Carbon Nitride Dots. *Nanoscale* **2020**, *12* (14), 7927–7938. <https://doi.org/10.1039/d0nr01647k>.
- (73) Bailey, R. L.; Dodd, K. W.; Gahche, J. J.; Dwyer, J. T.; McDowell, M. A.; Yetley, E. A.; Sempos, C. A.; Burt, V. L.; Radimer, K. L.; Picciano, M. F. Total Folate and Folic Acid Intake from Foods and Dietary Supplements in the United States: 2003-2006. *Am. J. Clin. Nutr.* **2010**, *91* (1), 231–237. <https://doi.org/10.3945/ajcn.2009.28427>.
- (74) Wu, X.; Suryoprabowo, S.; Kuang, H.; Liu, L. Detection of Aminophylline in Serum Using an Immunochromatographic Strip Test. *Food Agric. Immunol.* **2020**, *31* (1), 33–44. <https://doi.org/10.1080/09540105.2019.1691508>.
- (75) Niyi Dada, S.; Hua, M. Theranostic Nanoparticles for Simultaneous Detection and Treatment of Cancer. *NASSP Bull.* **1994**, *78* (559), 9–9. <https://doi.org/10.1177/019263659407855905>.
- (76) Yuan, Y.; Guo, B.; Hao, L.; Liu, N.; Lin, Y.; Guo, W.; Li, X.; Gu, B. Doxorubicin-Loaded Environmentally Friendly Carbon Dots as a Novel Drug Delivery System for Nucleus Targeted Cancer Therapy. *Colloids Surfaces B Biointerfaces* **2017**, *159*, 349–359. <https://doi.org/10.1016/j.colsurfb.2017.07.030>.
- (77) Bart, J.; Tiggelaar, R.; Yang, M.; Schlautmann, S.; Zuilhof, H.; Gardeniers, H. Room-Temperature Intermediate Layer Bonding for Microfluidic Devices. *Lab Chip* **2009**, *9* (24), 3481–3488. <https://doi.org/10.1039/b914270c>.
- (78) Gem, K.; Pc, H. C. L. Formulation and Evaluation of Gemcitabine HCl Loaded Phytosomes for Oral Drug Delivery. **2020**, *17* (3), 325-343.

- (79) Kaur, T.; Kaur, S.; Kaur, P. Development and Validation of UV-Spectrophotometric Methods for Determination of Gemcitabine Hydrochloride in Bulk and Polymeric Nanoparticles. *Int. J. Appl. Pharm.* **2017**, *9* (5), 60–65.
<https://doi.org/10.22159/ijap.2017v9i5.19726>.
- (80) Gao, N.; Yang, W.; Nie, H.; Gong, Y.; Jing, J.; Gao, L.; Zhang, X. Turn-on Theranostic Fluorescent Nanoprobe by Electrostatic Self-Assembly of Carbon Dots with Doxorubicin for Targeted Cancer Cell Imaging, in Vivo Hyaluronidase Analysis, and Targeted Drug Delivery. *Biosens. Bioelectron.* **2017**, *96* (January), 300–307.
<https://doi.org/10.1016/j.bios.2017.05.019>.
- (81) Pandey, S.; Thakur, M.; Mewada, A.; Anjarlekar, D.; Mishra, N.; Sharon, M. Carbon Dots Functionalized Gold Nanorod Mediated Delivery of Doxorubicin: Tri-Functional Nano-Worms for Drug Delivery, Photothermal Therapy and Bioimaging. *J. Mater. Chem. B* **2013**, *1* (38), 4972–4982. <https://doi.org/10.1039/c3tb20761g>.
- (82) Pandey, S.; Thakur, M.; Mewada, A.; Anjarlekar, D.; Mishra, N.; Sharon, M.; Yuan, Y.; Guo, B.; Hao, L.; Liu, N.; Lin, Y.; Guo, W.; Li, X.; Gu, B. Doxorubicin-Loaded Environmentally Friendly Carbon Dots as a Novel Drug Delivery System for Nucleus Targeted Cancer Therapy. *Colloids Surfaces B Biointerfaces* **2017**, *159* (38), 349–359.
<https://doi.org/10.1016/j.colsurfb.2017.07.030>.
- (83) Feng, T.; Ai, X.; An, G.; Yang, P.; Zhao, Y. Charge-Convertible Carbon Dots for Imaging- Cancer Therapeutic Efficiency Guided Drug Delivery with Enhanced in Vivo. *ACS Nano* **2016**, *10* (4), 4410–4420. <https://doi.org/10.1021/acsnano.6b00043>.
- (84) Yang, L.; Wang, Z.; Wang, J.; Jiang, W.; Jiang, X.; Bai, Z.; He, Y.; Jiang, J.; Wang, D.;

- Yang, L. Doxorubicin Conjugated Functionalizable Carbon Dots for Nucleus Targeted Delivery and Enhanced Therapeutic Efficacy. *Nanoscale* **2016**, 8 (12), 6801–6809.
<https://doi.org/10.1039/c6nr00247a>.
- (85) Vigevani, A.; Williamson, M. J. Doxorubicin; Academic Press, 1981; pp 245–274.
[https://doi.org/10.1016/S0099-5428\(08\)60143-4](https://doi.org/10.1016/S0099-5428(08)60143-4).
- (86) Dhenadhayalan, N.; Lin, K. C.; Suresh, R.; Ramamurthy, P. Unravelling the Multiple Emissive States in Citric-Acid-Derived Carbon Dots. *J. Phys. Chem. C* **2016**, 120 (2), 1252–1261. <https://doi.org/10.1021/acs.jpcc.5b08516>.
- (87) Han, J.; Na, K. Transfection of the TRAIL Gene into Human Mesenchymal Stem Cells Using Biocompatible Polyethyleneimine Carbon Dots for Cancer Gene Therapy. *J. Ind. Eng. Chem.* **2019**, No. 80, 420–743. <https://doi.org/10.1016/j.jiec.2019.02.015>.
- (88) Shen, S.; Wu, Y.; Liu, Y.; Wu, D. High Drug-Loading Nanomedicines : Progress , Current Status , and Prospects. *Int. J. Nanomedicine* **2017**, 12 (2017), 4085–4109.
<https://doi.org/https://dx.doi.org/10.2147%2FIJN.S132780>.
- (89) Park, C. M.; Xian, M. Use of Phosphorodithioate-Based Compounds as Hydrogen Sulfide Donors. *Methods Enzymol.* **2015**, 554 (2015), 127–142.
<https://doi.org/10.1016/bs.mie.2014.11.032>.
- (90) Bendale, Y.; Bendale, V.; Paul, S. Evaluation of Cytotoxic Activity of Platinum Nanoparticles against Normal and Cancer Cells and Its Anticancer Potential through Induction of Apoptosis. *Integr. Med. Res.* **2017**, 6 (2), 141–148.
<https://doi.org/10.1016/j.imr.2017.01.006>.

APPENDICES

Appendix A: Standard Calibration and Drug Release Tables

Table 4. Different Concentration/mg/mL of DOX and Absorbance Taken at 485nm

Concentration (mg/mL)	Absorbance
0.075	1.486
0.05	1.074
0.025	0.51
0.01	0.141
0.005	0.053
0.001	0.002
Blank	0

Table 5. Different Concentrations of GEM.HCl and Absorbance Measured at 269 nm

Concentration (mg/mL)	Absorbance at 268 nm
0.03	2.624
0.02	1.694
0.01	0.87
0.003	0.464
0.002	0.241
0.001	0.088
0	0

Table 6. The Concentration of DOX and the Cumulative Drug Release (CDR) in Dialysis
Medium from Noncovalent FA-CDs-DOX at pH 5.0

Sr No.	Time (hrs.)	Abs (A)	Conc. (mg/ml)	Amt. (mg)	CDR (%) pH 5.0
1	1	0.006	0.00145	0.145	14.51
2	2	0.021	0.00218	0.218	21.76
3	4	0.042	0.00319	0.319	31.92
4	7	0.045	0.00334	0.334	33.37
5	12	0.057	0.00392	0.392	39.18
6	22	0.066	0.00435	0.435	43.53
7	46	0.081	0.00508	0.508	50.78
8	72	0.126	0.00726	0.726	72.55

Table 7. The Concentration of DOX and the Cumulative Drug Release (CDR) in Dialysis
Medium from Noncovalent FA-CDs-DOX at pH 7.4

Sr No.	Time (hrs.)	Abs (A)	Conc. (mg/ml)	Amt. (mg)	CDR (%) pH 7.4
1	1	0.001	0.00121	0.121	12.09
2	2	0.006	0.00145	0.145	14.51
3	4	0.01	0.00164	0.164	16.44
4	7	0.012	0.00174	0.174	17.41
5	12	0.016	0.00194	0.194	19.35
6	22	0.017	0.00198	0.198	19.83
7	46	0.019	0.00208	0.208	20.80
8	72	0.023	0.00227	0.227	22.73

Table 8. The Concentration of DOX and the Cumulative Drug Release (CDR) in Dialysis
Medium from Noncovalent FA-CDs-DOX at pH 7.4

Sr No.	Time (hrs.)	Abs (A)	Conc. (mg/ml)	Amt. (mg)	CDR (%) pH 7.4
1	1	0.015	0.00074	0.0740	7.40
2	2	0.035	0.00130	0.1294	12.95
3	4	0.038	0.00138	0.1378	13.78
4	7	0.046	0.00160	0.1599	15.99
5	12	0.047	0.00163	0.1627	16.28
6	22	0.06	0.00199	0.1987	19.88
7	46	0.073	0.00235	0.2348	23.48
8	72	0.084	0.00265	0.2653	26.53

Example of Noncovalent CDs-DOX

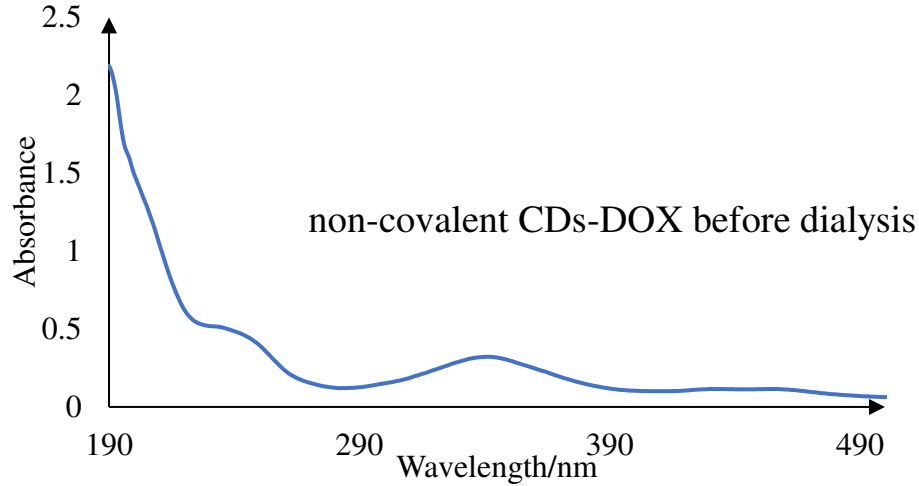


Figure 27. UV-vis of noncovalent CDs-DOX before dialysis.

DOX absorbance at 450 nm is 0.075. According to the equation of $Y = 20.676X - 0.0237$, the concentration of free DOX is 0.0048 mg/mL.

$$\text{Free DOX after synthesis} = 0.0048 \text{ mg/ml} \times 3.9 \text{ mL} = 0.01872 \text{ mg}$$

$$\text{Dilution factor (0.2 ml in 5 ml D.I water)} = 1/0.2 = 5$$

$$\text{Therefore, the mass of free DOX in the diluted sample} = 0.01872 \text{ mg} \times 5 = 0.0936 \text{ mg}$$

$$\text{The mass of total DOX for synthesis} = 1 \text{ ml} \times 0.4 \text{ mg/mL} \times 543.52/580 = 0.3748 \text{ mg}$$

$$\text{Therefore, the mass of DOX in conjugation after synthesis} = 0.3748 \text{ mg} - 0.0936 \text{ mg} = 0.2812 \text{ mg}$$

$$\text{DLE} = (0.2812 \text{ mg} / 0.3748) \times 100\% = 75.0\%$$

$$\text{DLC} = 0.28120 \text{ mg} / 4 \text{ mg} \times 100\% = 7.03 \%$$

Example of Noncovalent FA-CDs-DOX

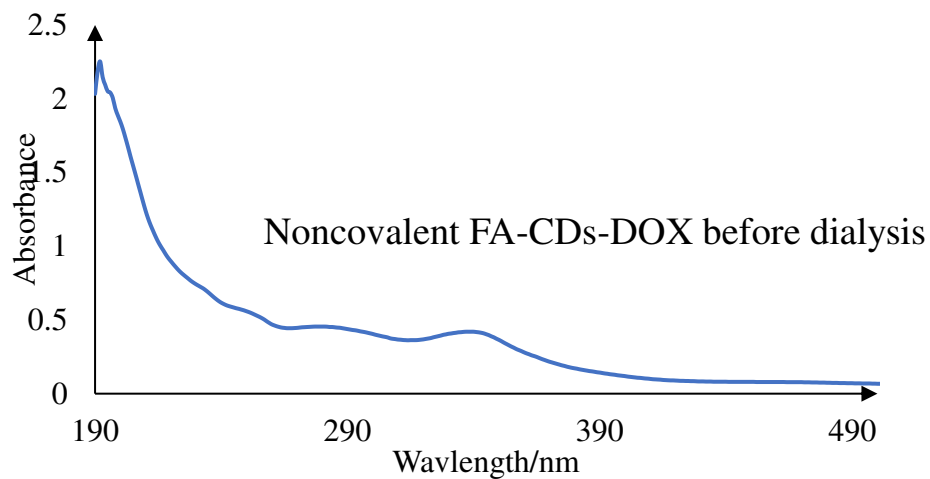


Figure 28. UV-vis of noncovalent FA-CDs-DOX before dialysis.

DOX absorbance at 485 nm is 0.072. According to the equation of $Y = 20.676X - 0.0237$, the concentration of free DOX is 0.00463 mg/ml

Dilution factor (0.2 ml in 5 ml D.I water) = $1/0.2 = 5$

Therefore, the mass of free DOX after synthesis = $0.00463 \text{ mg/ml} \times 3.9 \text{ mL} \times 5 = 0.0903 \text{ mg}$

The mass of total DOX for synthesis = $1.0345 \text{ } \mu\text{mol} \times 543.52 = 0.5623 \text{ mg}$

Mass of DOX in conjugation after synthesis = $0.5623 \text{ mg} - 0.0978 \text{ mg} = 0.472 \text{ mg}$

DLE = $0.472 \text{ mg} / 0.5623 \text{ mg} \times 100\% = 83.8\%$

DLC = $0.472 \text{ mg} / (8 \text{ mg/ml} \times 1.5 \text{ ml}) \times 100\% = 3.9\%$

Example of Covalent FA-CDs-DOX

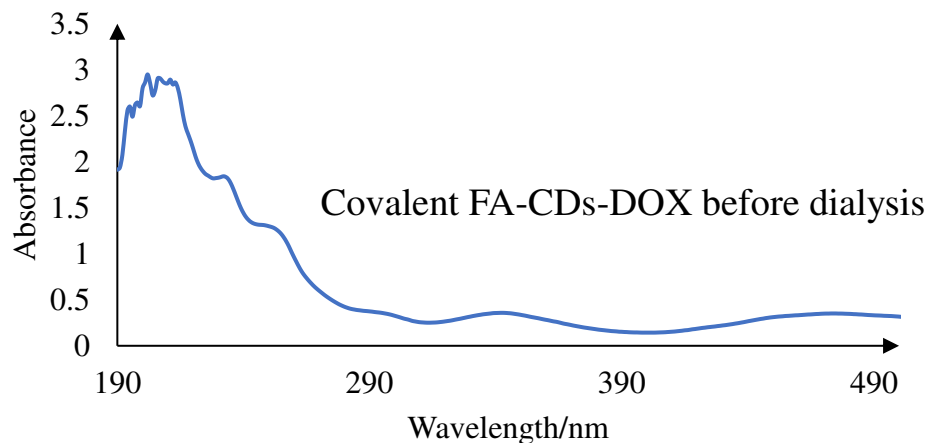


Figure 29. UV-vis of covalent FA-CDs-DOX before dialysis

DOX absorbance at 485 nm is 0.340, According to the equation of $Y = 20.676X - 0.0237$, the concentration of free DOX is 0.0175 mg/mL.

The dilution factor = $0.2\text{ml}/5\text{ml} = 25$.

Free DOX after synthesis = $0.0175\text{mg/ml} \times 25 \times 3\text{ mL} = 1.3125\text{ mg}$

The mass of total DOX for synthesis = $8.36\text{ uMol} \times 543.5\text{g/mol} = 4.54\text{ mg}$

Mass of DOX in conjugation after synthesis = $4.54\text{ mg} - 1.3125\text{mg} = 3.2275\text{ mg}$

DLE = $(3.2275\text{ mg} / 4.54) \times 100\% = 71.0\%$

DLC = $3.32591\text{mg} / (4\text{mg CDs} + 0.013\text{mg FA}) \times 100\% = 80\%$

Example of Covalent CDs-DOX

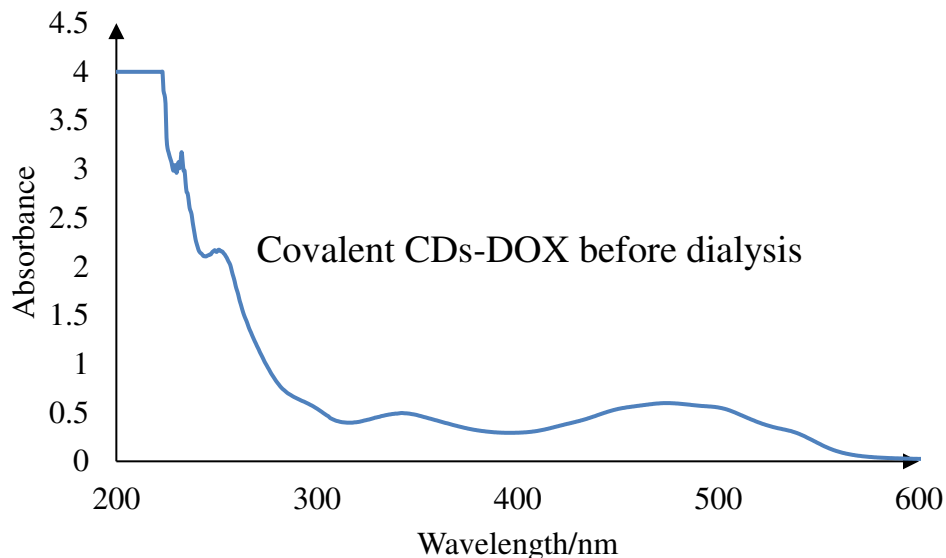


Figure 30. UV-vis of covalent CDs-DOX before dialysis.

DOX absorbance at 485 nm is 0.582. According to the equation of $Y = 20.676X - 0.0237$, the concentration of free DOX is **0.029mg/mL**

Free DOX after synthesis = $0.029 \text{ mg. ml} \times 2.9 \text{ mL} = 0.0841 \text{ mg}$

Dilution factor (0.2 ml in 5 ml D.I water) = $5/0.2 = 25$

Therefore, the mass of free DOX in the diluted sample = $0.0841 \text{ mg} \times 25 = 2.102 \text{ mg}$

The mass of total DOX for synthesis = $8.36 \mu\text{mol} \times 543.5 \text{ g/mol} = 4.54 \text{ mg}$

Mass of DOX in conjugation after synthesis = $4.54 \text{ mg} - 2.102 \text{ mg} = 2.438 \text{ mg}$

DLE = $(2.438/4.54) \times 100\% = 53.7\%$

DLC = $2.8853 \text{ mg} / (4 \text{ mg CDs}) \times 100\% = 60.9 \%$

Example of Covalent CDs-GEM.

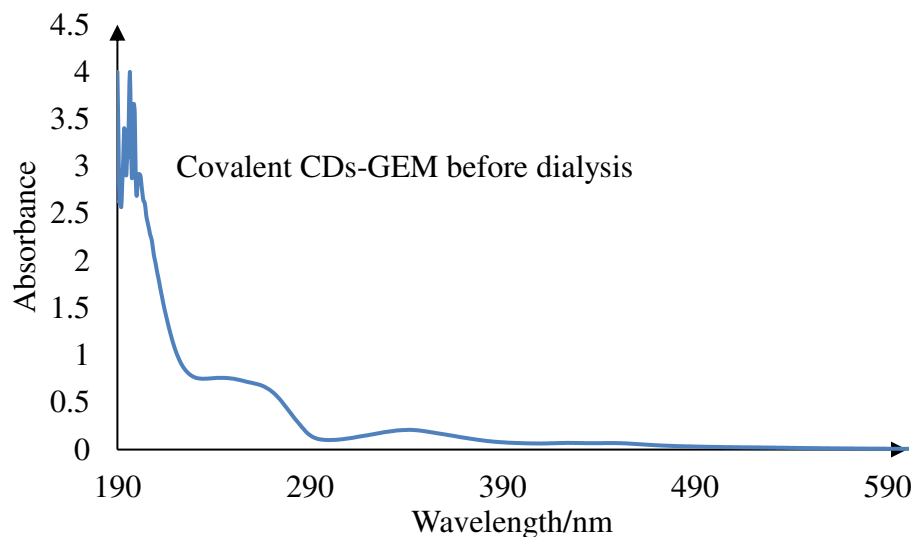


Figure 31. UV-vis of covalent CDs-GEM before dialysis.

GEM.HCl absorbance at 269 nm is 0.634. According to the equation of $Y = 83.637X - 0.0608$, the concentration of free GEM.HCl is 0.00831 mg/mL

Free GEM.HCl after synthesis = $0.00831 \text{ mg/mL} * 3 \text{ mL} * 25 = 0.6231 \text{ mg}$

The mass of GEM.HCl after synthesis = $5 \text{ mg/ml} * 0.5 \text{ mL} = 2.5 \text{ mg}$

Mass of GEM.HCl in conjugation after synthesis = $2.5 \text{ mg} - 0.6231 \text{ mg} = 1.8769 \text{ mg}$

$\text{DLE} = 1.8769 \text{ mg} / (5 \text{ mg/ml} * 0.5 \text{ ml}) * 100\% = 75.1$

Mass of CDs used in the synthesis = 4 mg

$\text{DLC} = 1.8769 \text{ mg} / (4) = 46.9 \%$

Example of Covalent FA-CDs-GEM.

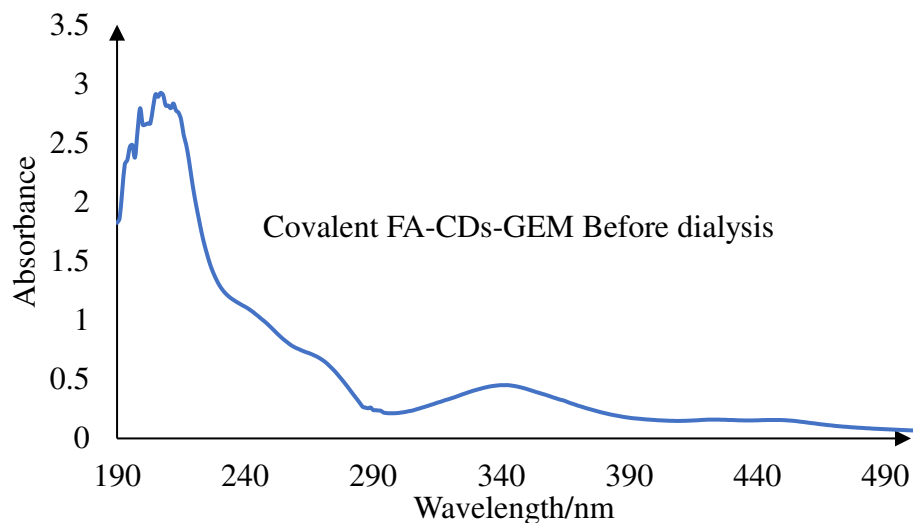


Figure 32. UV-vis of covalent FA-CDs-GEM before dialysis.

GEM absorbance at 269 nm is **0.68**. According to the equation of $Y = 83.637X - 0.0608$, the concentration of free GEM.HCl is **0.00982 mg/mL**

Free GEM after synthesis = $0.00886 \text{ mg/mL} * 3 \text{ mL} * 25 = \mathbf{0.664 \text{ mg}}$

The mass of GEM.HCl after synthesis = $5 \text{ mg/mL} * 0.5 \text{ mL} = 2.5 \text{ mg}$

Mass of GEM after synthesis (when HCl is no more bonded to GEM) = $8.3 \mu\text{Mol} * 263.2 \text{ mg/mole} = \mathbf{2.184 \text{ mg}}$

Therefore, the mass of GEM in conjugation after synthesis = $2.184 \text{ mg} - 0.664 \text{ mg} =$

1.5197 mg

$\text{DLE} = 1.5197 \text{ mg} / (2.184 \text{ mg}) * 100\% = 69.6\%$

Mass of CDs used in the synthesis = 4 mg

Mass of folic acid used for the synthesis = 0.013 mg

The total mass of FA and CDs = 4.013 mg

$$\text{DLC} = 1.5197 \text{ mg} / 4.013 * 100 = \mathbf{37.8\%}$$

VITA

GODWIN KWEKU BABANYINAH

- Education: M.S. Chemistry, East Tennessee State University, Johnson
City, Tennessee, 2021
- B.Sc. Biochemistry, University of Cape Coast, Cape Coast, Ghana,
2018
- Professional Experience: Graduate Assistant, East Tennessee State University, College of
Arts and Sciences, 2019-2021
- Teacher Assistant; University of Cape Coast, Ghana, 2018-2019
- Clinical Laboratory Assistant. Saltpond Municipal Hospital,
Ghana, Jun 2017– Sep 2017
- Publications: Boison, D.; Adinortey, C. A.; Babanyinah, G. K.; Quasie, O.;
Agbeko, R.; Wiabo-Asabil, G. K.; Adinortey, M. B. Costus Afer:
A Systematic Review of Evidence-Based Data in Support of Its
Medicinal Relevance. *Scientifica (Cairo)*. 2019, 2019, 1–10.
<https://doi.org/10.1155/2019/3732687>
- Honors and Awards: Appalachian Student Research Forum, 2021
- ACS Spring National Conference/Meeting, 2021
- 3 Minute Thesis Competition, 2020